January 2018

# Synthesis And Characterization Of Novel Ternary Borides (MoAlB) And Their Composites

Matt Fuka

# SYNTHESIS AND CHARACTERIZATION OF NOVEL TERNARY BORIDES (MoAlB) AND THEIR COMPOSITES

by

Matt Ryan Fuka

Bachelor of Science, University of North Dakota, 2015

A Thesis

Submitted to the Graduate Facility

of the

University of North Dakota

In partial fulfillment of the requirements

For the degree of

Master of Science

Grand Forks, North Dakota

May

2018

This thesis, submitted by Matt Ryan Fuka in partial fulfillment of the requirements for the Degree of Master of Science from the University of North Dakota, has been read by the Faculty Advisory Committee under whom the work has been done and is hereby approved.

_____

Dr. Surojit Gupta, Ph.D.

_____

Dr. Clement Tang, Ph.D.

_____

Dr. Cai Xia Yang, Ph.D.

This thesis meets the standards for appearance, conforms to the style and format requirements of the School of Graduate Studies at the University of North Dakota, and is hereby approved.

_____

Grant McGimpsey

Dean of the School of Graduate Studies

_____

Date

# PERMISSION

| | |
|---|---|
| Title | Synthesis and Characterization of Novel Ternary Borides (MoAlB) and Their Composites |
| Department | Mechanical Engineering |
| Degree | Master of Science |

In presenting this thesis in fulfillment of the requirements for a graduate degree from the University of North Dakota, I agree that the library of this University shall make it freely available for inspection. I further agree that permission for extensive copying for scholarly purposes may be granted by the professor who supervised my thesis work or, in his absence, by the chairperson of the department or the dean of the School of Graduate Studies. It is understood that any copying or publication or other use of this thesis or part thereof for financial gain shall not be allowed without my written permission. It is also understood that due recognition shall be given to me and to the University of North Dakota in any scholarly use which may be made of any material in my thesis.

Signature Matt Ryan Fuka

Date

TABLE OF CONTENTS

## LIST OF FIGURES

# LIST OF TABLES

## ACKNOWLEDGEMENTS

I am grateful to my colleagues, Sujan Ghosh, Faisal AlAnazi, and Maharshi Dey. I would also like to express my sincerest gratitude to Dr. Surojit Gupta at the University of North Dakota for all of the aid and guidance I received during my studies. For without them, this work would not have been possible.

In addition, I would like to thank all the professors at the University of North Dakota who have taught me along the way and my friends and family who have helped me throughout my studies.


Trust in the LORD with all your heart and lean not on your own understanding; in all your ways submit to him, and he will make your paths straight.

- Proverbs 3:5-6

# ABSTRACT

This work details the synthesis and characterization of novel ternary boride (MoAlB) and MAX phase particulates via pressureless reaction. Furthermore, porous MoAlB particulates were synthesized for the first time by selective deintercalation of Al from MoAlB. Finally, novel Ni-MoAlB composites were fabricated, and their mechanical and tribological properties were tested and analyzed. Chapter II describes the synthesis of $Cr_2AlC$, $Cr_2GaC$, and $V_2AlC$ powders, and demonstrates the ability to engineer particle size of $Ti_3SiC_2$ by ball milling. Chapter III details the synthesis and characterization of a novel ternary boride, MoAlB, and their porous derivatives. These particulates showed a uniquely stacked 2D-like morphology and were riddled with pores of dimensions 257±126 nm and 35±10 nm, respectively. The EDS analysis showed that particulates had a chemistry of $(Mo_{0.67}Al_{0.33})B\{O_{0.19}F_{0.02}\}$ due to partial deintercalation of Al from MoAlB. Chapter IV chronicles the fabrication of novel Ni-matrix composites using MoAlB powders as a multifunctional solid lubricant additive. During sliding against SS, the WR decreased gradually with MoAlB content, for example, it decreased from 3 x $10^{-3}$ $mm^3/Nm$ in Ni (240 MPa) to ~2 x $10^{-4}$ $mm^3/Nm$ in Ni-30%MoAlB (1000 °C) (240 MPa). Chapter V discusses the conclusions and future studies of this work.

# CHAPTER I

# INTRODUCTION

## 1.1 Lubrication

In today's modern society there are an extensive amount of applications which utilize the sliding of two surfaces over each other, e.g. pistons in an engine or bearings in a wheel. Typically, liquid lubricants are used to reduce friction and increase useful life of the part; however, this requires periodical replacement of the lubricants, and are sometimes not a practical option if the operating environment will subject the lubricants to extreme temperatures and pressures. Because the relationship between viscosity of fluid lubricants and temperature is very significant, it is essential that the operating temperature of the part is kept within the design range of the selected fluid lubricant [1, 2]. As temperature increases, the viscosity of the fluid significantly drops, and conversely as temperature decreases, the viscosity significantly increases. Furthermore, the relationship between fluid lubricants and pressure is also a crucial component of fluid lubrication. Increases in pressure will result in increases in viscosity and the lubricant may lose some of its liquid properties and behave more like a wax [1]. But if the pressure drops below the fluid vapor pressure, the fluid will unstably rupture and instantaneously cavitate [2]. Thus it is imperative that the operating temperatures and pressures match the design specifications, otherwise it will lead to early part failure. However, in some cases, extreme environments are unavoidable and in fact the objective (e.g. space exploration), and in such situations solid lubricants are a viable option for lubrication.

Solid lubricants are defined as a functional material which can significantly decrease the frictional force between two surfaces sliding against one another. The mating surfaces are known as a tribocouple, and the tribological properties of the system are dependent on various factors such as temperature, chemical composition, applied load, sliding speed, and sliding distance. Solid lubricants reduce friction and wear of tribocouples typically by formation of tribofilms, which are thin films adherent to the surface of the material and provide lubricious properties greatly impacting the friction and wear behaviors of the mating materials [3]. Solid lubricants are advantageous over liquid lubricants because they can be used when: expected loads are high, operating speeds are low, operating temperatures are extreme, and operating environments are dirty or extreme, as well as a variety of other reasons [4].

While traditional solid lubricants (e.g. graphite and molybdenum disulfide) have advantageous lubricating properties because of their lamellar structure, they are most often used in a powder form and thus do not maximize their tribological capabilities. To optimize the use of solid lubricants, the solid lubricant must be bonded to the surface of which it is lubricating. From Clauss [4], it is shown that solids impregnated with solid lubricants possess enhanced tribological properties; however, drawbacks to traditional solid lubricants are relatively low oxidation temperatures, relatively soft, and they do not offer many other advantageous properties than tribological [5]. Furthermore, as space exploration efforts are expanded and working times of mechanical systems in space are increased, space tribology is an important issue that needs to be addressed. Mechanical systems in space are exposed to an environment with low pressure, radiation, atomic oxygen and no gravitation [1]. While $MoS_2$ is currently widely used in coatings for tribocouples in space, composite material performance must be improved to increase the

overall performance of the space vehicle. Thus, a need was realized for a next generation material that could provide composites with improved mechanical, chemical, and tribological properties.

### 1.2 MAX Phases

A novel class of materials called MAX phases were first reported developed in the 1970's by Nowotny; however, they were for the most part ignored, and it wasn't until the early 2000's that interest in MAX phases broke out [6]. MAX phases are a family of layered, hexagonal, early transition-metal ternary carbides and nitrides. Their chemical formula is $M_{n+1}AX_n$, where n = 1, 2, or 3, M is an early transition metal, A is a group A element, and X is carbon or nitrogen (Fig. 1.1) [7].

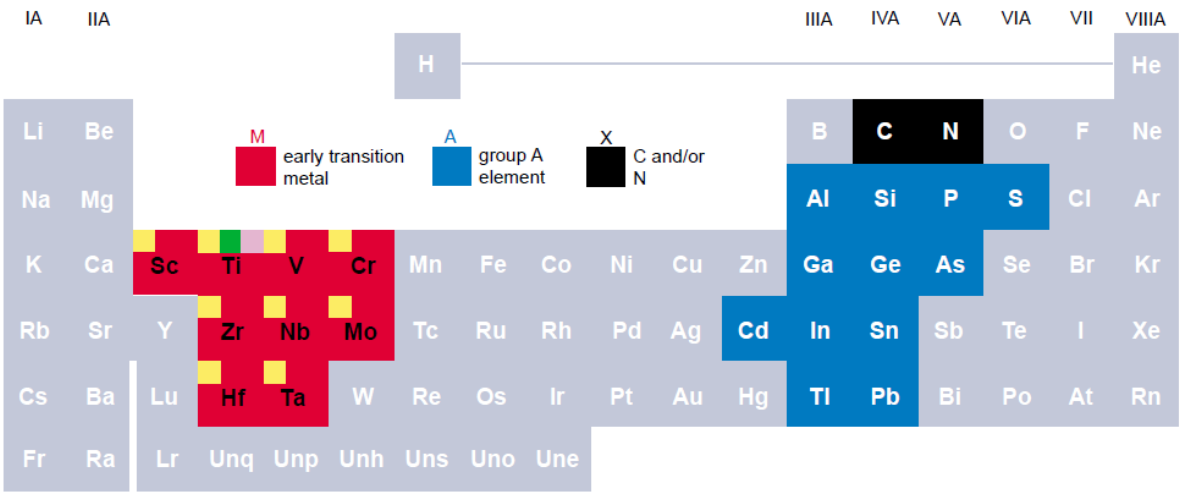


Figure 1.1: MAX phases are made up of M – early transition metal (red), A – element from the A groups (blue), and X – carbon or nitrogen (black). Their chemical formula is $M_{n+1}AX_n$, where n = 1, 2, or 3, and each respective group is known as 211, 312, or 413 [7].

A unique feature of MAX phases is that they possess characteristics of both metals and ceramics. An example of a widely studied MAX phase exhibiting superior properties of both metals and ceramics is $Ti_3SiC_2$. Notable metallic properties of this MAX phase are excellent thermal and electrical conductivity, easily machinable, relatively soft, resistant to thermal shock,

and plastic behavior at higher temperatures. Yet, like a ceramic, $Ti_3SiC_2$ is oxidation resistant, extremely refractory, and able to maintain strength at elevated temperatures [8]. Furthermore, Gupta et al. [9-11] has shown that MAX phases have favorable tribological behaviors in dry sliding at ambient and elevated temperatures. This special class of materials shows great promise in delivering the essential mechanical, chemical, and tribological properties for next generation composites and coatings, and thus can be considered for a variety of applications such as in heating elements, tooling and drilling, high-temperature foil bearings, electrical contacts, and an array of other applications.

### 1.3 MXenes

Recently, a unique two-dimensional variant of MAX phases, called MXenes, were first reported discovered in 2011 by Naguib et al. [12]. Similar to MAX phases, MXenes are layered, hexagonal, ternary carbides and nitrides; however, the "A" element has been removed and the "$M_{n+1}X_n$" layers are instead loosely bound by hydrogen or van der Waals bonds. The chemical formula of the etched layers is $M_{n+1}X_nT_x$, where T represents the different surface terminations based on etching solution chemistry [13]. These loosely bound layers can then be exfoliated into individual nanometer thick crystalline layers, akin to graphene, and can roll into conical shapes with radii of less than 20 nm. A significant feature of MXenes is that their electronic properties can be tuned by changing their surface terminations. Because of MXenes distinctive structural and chemical characteristics, it makes them very promising candidates for a variety of applications, such as in structural composites, water purification, lubrication, and most notably for energy transport and storage [12-14].

### 1.4 MAB Phases

In 1997, Okada et al. first reported single crystal synthesis of MoAlB and WAlB, and the respective chemical and physical properties of these new phases of materials [15]. In 2015, Ade and Hillebrecht [16] reported single crystal synthesis of other various ternary borides including: $Cr_2AlB_2$, $Cr_3AlB_4$, $Cr_4AlB_6$, MoAlB, WAlB, $Mn_2AlB_2$, and $Fe_2AlB_2$, as well as the various crystal structures of each respective ternary boride. The authors noticed their similarity to MAX phases and hence named them MAB phases. MAB phases are layered, ternary transition metal borides with intriguing material properties (e.g. extremely high thermal, chemical, and mechanical stability) resulting from the corresponding binary borides. MAB phases are very similar to MAX phases in that they have alternating layers of ceramic and intermetallic subunits, and it is this anisotropic structure that lends to their unique properties. However, unlike MAX phases, there are a much more limited set of MAB phases, but their crystal structures are more distinct and complex dependent on the composition of the MAB phase. The complexity of MAB phases lends to the fact that there are three variables to their structures: thickness of the boride component, number of metal layers inbetween the boride layers, and the orientation of the boron subunits. In comparison, MAX phases have only one variable: the thickness of the carbide component, which is then interleaved by one metal "A" layer.

A particular MAB phase that has recently been of research interest is MoAlB, which has an orthorhombic crystal structure and is of the space group *Cmcm* [16]. Kota et al. [17] reported the synthesis and characterization of MoAlB (Fig. 1.2) via reactive hot-pressing, and hypothesized that a passivating alumina layer would form upon heating in air because of its close structural similarity to MAX phases and its high Al content.

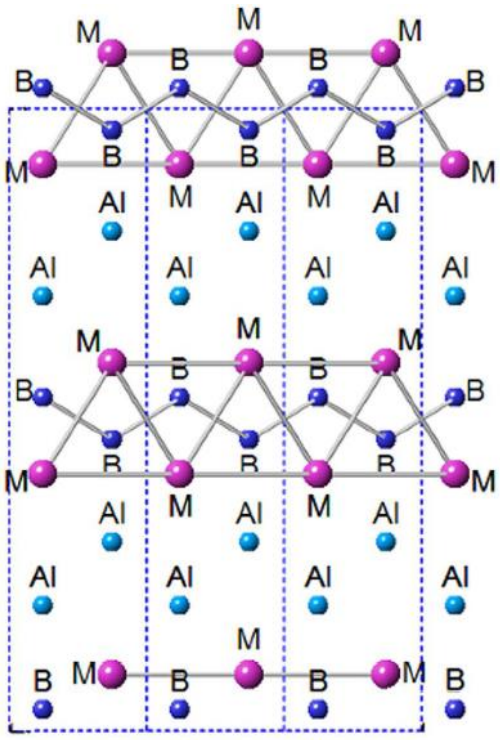


Figure 1.2: Crystal structure of MoAlB [17].

The researcher's hypothesis was confirmed as indeed a passivating, mostly amorphous, alumina layer was formed upon heating in inert atmospheres, thus giving MoAlB stability in temperatures as high as 1400 °C. Kota et al. also report low electrical resistivity (0.36 – 0.49 μΩm), good thermal conductivity (35 $Wm^{-1}K^{-1}$ at 26 °C), thermal expansion coefficient of 9.5 x $10^{-6}K^{-1}$ (from 25-1300 °C), moderately low Vickers hardness (10.6 ± 0.3 GPa) compared with other transition metal borides, and an ultimate compressive strength of 1940 ± 103 MPa at room temperature. The author states that because of these encouraging results, further study is warranted on MoAlB for potential use at high temperatures. This thesis will focus on synthesis and characterization of novel MoAlB particulates, their porous derivatives, and their use as a multifunctional solid lubricant.

### 1.5 MAX Reinforced Metals (MRMs)

MAX reinforced metals (MRMs) are metal matrix composites reinforced with MAX phase particulate reinforcement dispersed throughout the metal matrix. Gupta et al. [18-23] has clearly shown that these composites enhance the mechanical and tribological performances of the pure metal matrix, and are very intriguing because of their ability to impart self-lubricity to the composite. This, among other favorable properties, makes MRMs viable candidates for applications where high mechanical and tribological performances of metal matrix composites are needed. Figures 1.3 & 1.4 below show the beneficial impacts of adding $Ti_3SiC_2$ to various metal matrices [22].

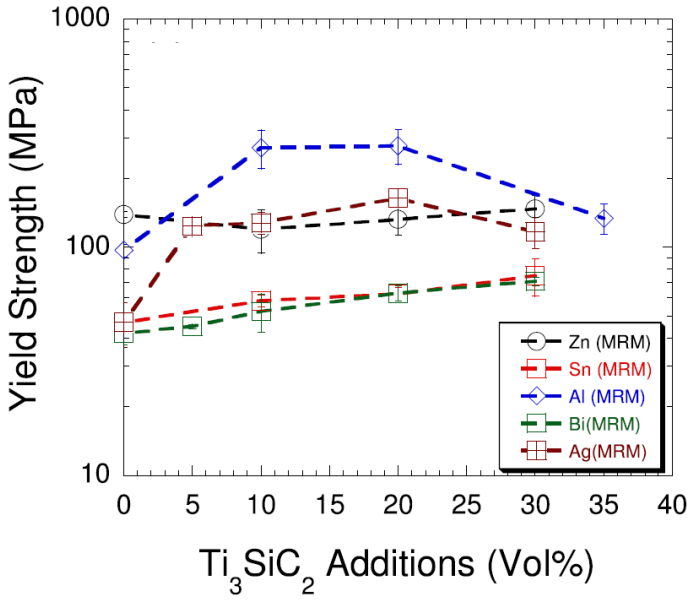


Figure 1.3: Plot of stress versus displacement of yield strength of different MRMs versus $Ti_3SiC_2$ content [22].

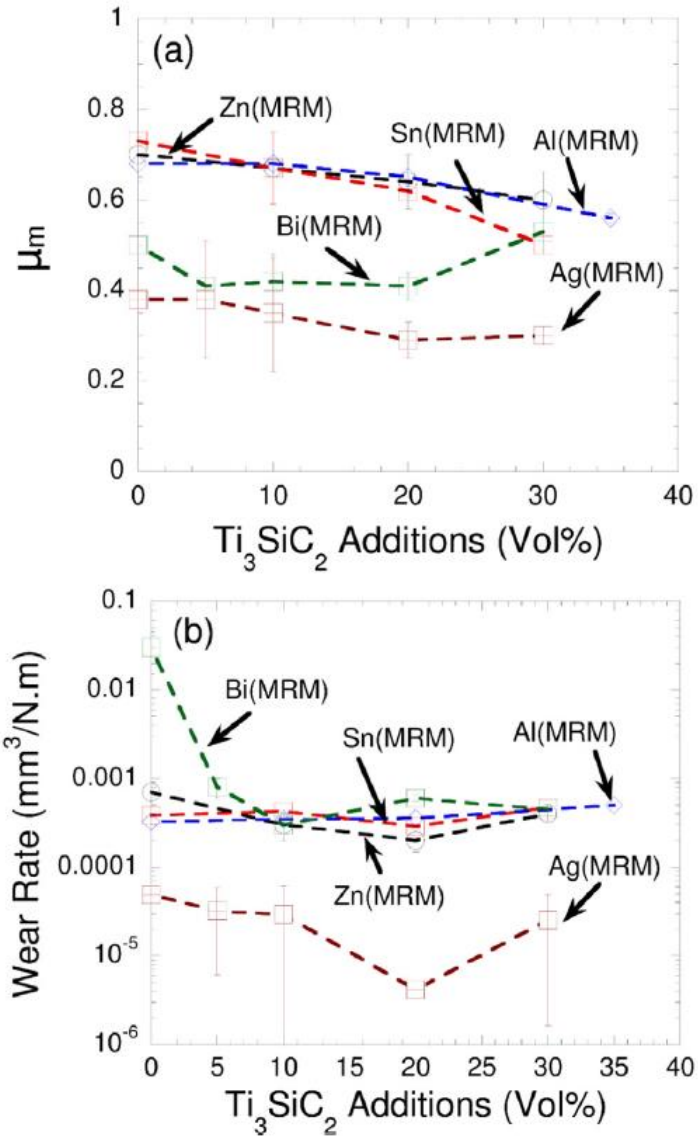


Figure 1.4: Plot of MRMs (a) $\mu_m$, and (b) wear rates as a function of $Ti_3SiC_2$ content [22].

Not only have MAX phases been shown to improve the mechanical and tribological performances in metal matrices, but Gupta et al. [24-26] has also shown them to do the same in polymer matrices. In such cases, these composites are called MAX reinforced polymers (MRPs), and their enhanced properties make MRPs viable candidates for applications where high mechanical and tribological performances of polymer matrix composites are needed. Figure 1.5 below shows the beneficial impacts of adding $Ti_3SiC_2$ to various polymer matrices [26].

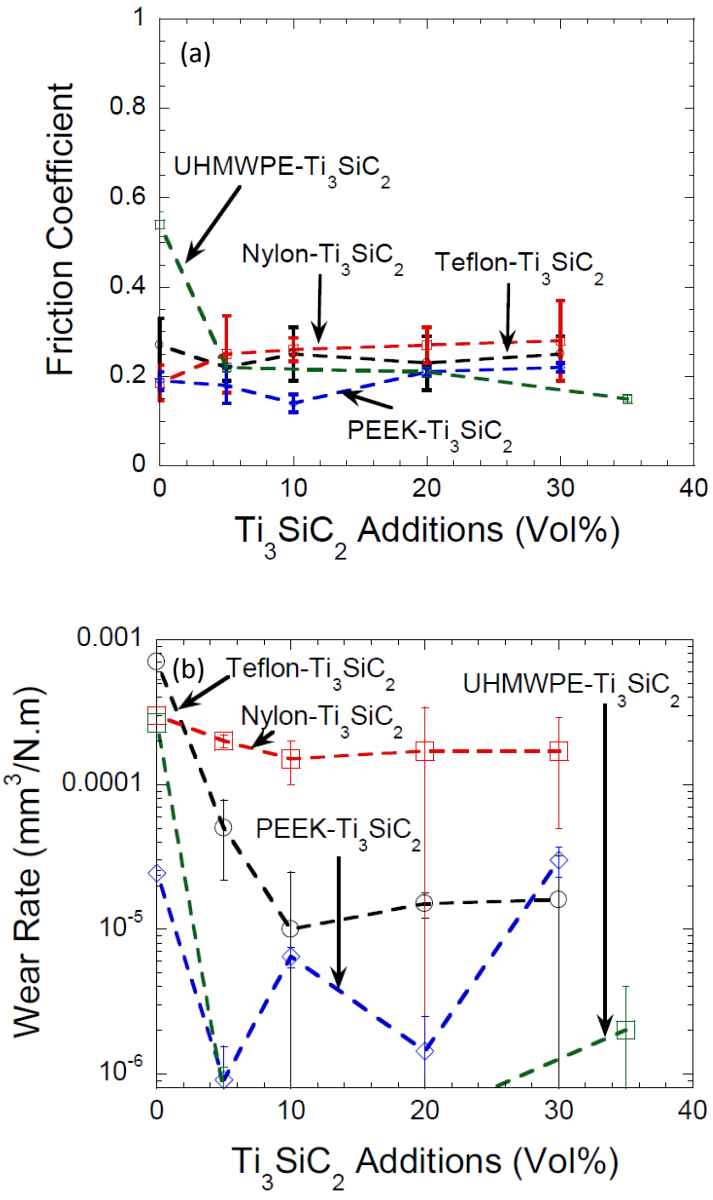


Figure 1.5: Plot of MRPs (a) $\mu_m$ and (b) wear rates as a function of $Ti_3SiC_2$ content [26].

### 1.6 Metals Reinforced with MAB (MRMB) and Porous MAB Derivatives

This thesis focuses on the development of MAX phase powders via pressureless reaction, the synthesis of novel MoAlB powders via pressureless reaction, the synthesis of novel porous MoAlB particulates, and the fabrication of Ni-MoAlB composites and their mechanical and tribological properties. To begin, various MAX phase particulates will be synthesized via

pressureless reaction and the particle size of $Ti_3SiC_2$ will be engineered by ball milling. The $Ti_3SiC_2$ particulates will be ball milled in a hardened steel vial with hardened steel balls for 30 minutes. To fabricate the $Cr_2AlC$, $Cr_2GaC$, and $V_2AlC$ powders, the required ratio of powders will be mixed in a methacrylate vial with methacrylate balls for 5 minutes, except for the $Cr_2GaC$ composition. For synthesis of $Cr_2GaC$ particulates, the required ratio of Cr and C will be dry milled for 5 minutes and thereafter the required amount of Ga will be added and mixed in a mortar and pestle for at least 15 minutes. All powders will then be cold pressed, sintered at different temperatures under flowing Ar gas, crushed in a ball mill, and sieved until -325 mesh in a sieve shaker. The powders will have XRD measurements performed to confirm single phase and SEM images will obtained.

Following this research, novel MoAlB particulates and their porous derivatives will be synthesized and characterized. MoAlB powders will initially be fabricated by mixing powders of MoB and Al in the required molar ratio and dry ball milling in a methacrylate vial with methacrylate balls for 5 minutes. The mixed powders will then be subsequently cold pressed, annealed at 750 °C for 2 hours, and heat treated at 1550 °C for 2 hours under flowing Ar gas. The sintered compacts will then be crushed in a ball mill, sieved until -325 mesh in a sieve shaker, and XRD analysis will be performed to confirm predominantly single phase MoAlB powders. Due to the close structural similarity between MAX and MAB phases [16], it is hypothesized that MoAlB can also be etched to form a MXene like MAB phase, and that fully etched MAB phases will hold similarly intriguing properties as those of MXenes. Therefore, after obtaining MoAlB powders, these particulates will be etched by treating with ~40 milliliters of 12 M HCl and 1 gram (~1 M) LiF. Ensuing the etching process, XRD and EDS analysis will be performed, and SEM images will be obtained on the etched MoAlB particulates.

Finally, Ni-matrix composites will be fabricated using MoAlB powders as a multifunctional solid lubricant additive. Because of previous studies showing enhanced mechanical and tribological behaviors with additions of MAX phases [18-23] and the similarities between MAX and MAB phases [16, 17], it is postulated that MoAlB particulates will have a similar effect on metal matrix composites. MoAlB powders will be fabricated in the same method as previously described, and these powders will then be dry ball milled with the required amount of Ni to make novel Ni-MoAlB composites. The mixed powders will then be hot-pressed under a uniaxial compressive stress at 600 °C for 5 minutes. In addition, pure Ni samples will be fabricated using the same procedure mentioned above for comparison. Relative density will be obtained for all samples, and theoretical density will be calculated using rule of mixtures. Compression testing will be conducted using a Shimadzu Ultimate Testing Machine, and hardness testing will be conducted using a Vickers micro-hardness indenter. Tribological behaviors of the composites will be tested using ball-on-disc and block-on-disc tribometer. After tribology testing, EDS analysis and SEM images will be obtained of the tribosurfaces.

# CHAPTER II

# DESIGN AND SYNTHESIS OF NOVEL NANO-LAMINATED PARTICULATES FOR FABRICATING NOVEL MULTIFUNTIONAL COMPOSITES

This work was published in International Journal of Innovative Research in Science Engineering and Technology, "Design and Synthesis of Novel Nano-laminated Particulates for Fabricating Novel Multifunctional Composites", M. Fuka, F. AlAnazi, S. Ghosh, and S. Gupta, IJIRSET, 2016, DOI:10.15680/IJIRSET.2016.0512138.

## 2.1 Introduction

$M_{n+1}AX_n$ (MAX) phases (over 60+ phases), where n =1,2,3; M is an Early Transitional Metal, A is a Group A element (mostly groups 13 and 14); and X is C and/or N, are novel ternary carbides or nitride which have attractive properties like damage tolerance, thermal shock resistance and machinability [1-5]. Recently, composites of MAX phases with different polymers and metals have attracted a lot of attention [6-13]. In order to further exploit these materials, it is critical to design and engineer novel MAX Phases particulates. The aim of this paper is to report the synthesis and characterization of novel particulates of $Ti_3SiC_2$, $Cr_2AlC$, $Cr_2GaC$, and $V_2AlC$.

## 2.2 Experimental Details

$Ti_3SiC_2$ powder (-325 mesh, Kanthal, Hallstahammar, Sweden) was ball milled (8000 M mixer Mill, SPEX SamplePrep, Metuchen, NJ) for 30 min in an 8001B hardened steel vial with 8001B hardened steel balls (Composition A). Table 2.1 shows the specifications of the powder

used during this study. For fabricating, (a) $Cr_2AlC$ (Composition B), a ratio of Cr:Al:C was 2:1.1:1, (b) $Cr_2GaC$ (Composition C), a ratio of Cr:Ga:C was 2:1.4:1, and (c) $V_2AlC$ (Composition D), a ratio of V:Al:C was 2:1.2:1, was used. The required ratio of powders were mixed in the ball milled in a methacrylate vial with methacrylate balls for 5 min except $Cr_2GaC$ (Composition C).

Table 2.1: Specification of the raw materials used during this study.

| Powders | Source | Specifications |
|---|---|---|
| Chromium | Part 266299, Sigma-Aldrich, St. Louis, MO | powder, ≥99% trace metal basis, -325 mesh |
| Vanadium | Part 262935, Sigma-Aldrich, St. Louis, MO | powder, 99.5% trace metal basis, -325 mesh |
| Aluminum | Lot KO5Z034, Alfa Aesar, Haverhill MA | powder, 99.5% trace metal basis, -325 mesh |
| Carbon | LotY19B065, Alfa Aesar, Haverhill MA | Graphite powder crystalline , 99%, -325 mesh |
| Gallium | 100 g, Rotometals Inc., San Leandro CA | 99.99% Ingot |

For synthesizing $Cr_2GaC$ particulates, the required ratio of Cr and C were dry milled for 5 min, thereafter required amount of Ga was added to the mixed powders, and thereafter it was mixed in a mortar and pestle for at least 15 minutes. All the powders were then cold pressed and subsequently sintered at different temperatures in a tube furnace with Ar gas flowing though the furnace. Compositions A and B were heated at 10 $^oC$/min to the desired temperature, whereas composition C was heated at 5 $^oC$/min to the desired temperature. The sintered powders were then crushed in a ball mill, and then sieved until -325 mesh in a sieve shaker. XRD measurements were performed by a Rigaku Diffractometer (SmartLab, Rigaku, Japan) at a scan rate of 0.05 $^o$/min from $20^o$ to $50^o$. For all samples, Secondary electron (SE) images were obtained by using a JEOL JSM-6490LV Scanning Electron Microscope (JEOL USA, Inc., Peabody, Massachusetts).

## 2.3 Results and Discussion

Figure 2.1 compares the XRD pattern of $Ti_3SiC_2$ after milling with as-received $Ti_3SiC_2$ (Composition A). By analyzing the XRD patterns of both the samples, we can conclude that there is no sign of oxidation in the milled samples. Figure 2.2 compares the SE SEM micrographs of $Ti_3SiC_2$ particulates before and after milling. By comparing the micrographs, we can conclude that ball milled powders have lower particle size as compared to as-received $Ti_3SiC_2$.

Figure 2.3 shows the XRD patterns of Composition B sintered at different temperatures. Significant amount of binary carbide ($Cr_7C_3$) was observed after sintering at 1300 $^oC$ for 1 h. The concentration of $Cr_7C_3$ decreased on heat treatment at 1300 $^oC$ for 4 h, and the peaks of $Cr_2AlC$ increased. On treatment at 1350 $^oC$ for 4 h, only peaks of $Cr_2AlC$ were observed. Thus, 1350 $^oC$ for 4 h can be used as an optimum temperature for synthesizing $Cr_2AlC$ powders.

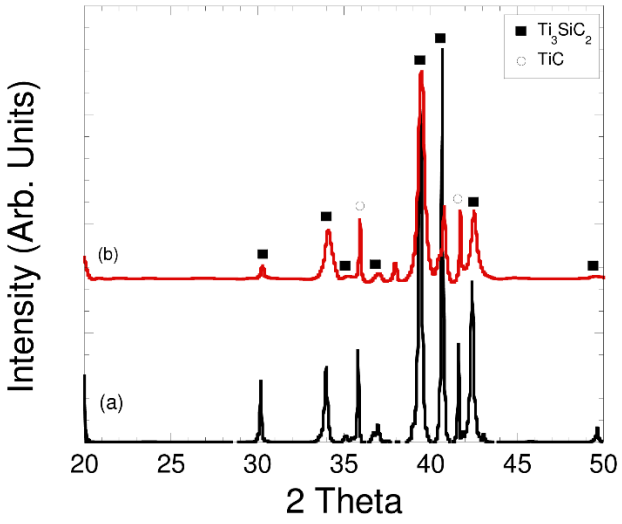


Figure 2.1: Plot of XRD patterns of, (a) $Ti_3SiC_2$ (as received), and (b) $Ti_3SiC_2$ ball milled for 30 min.

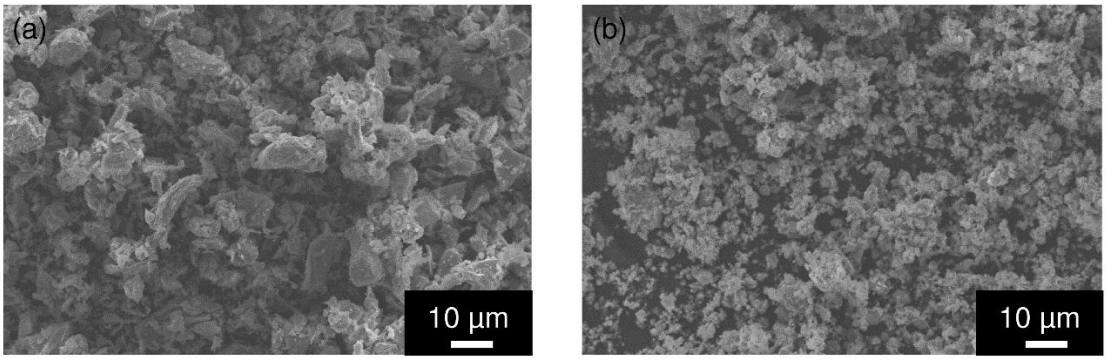


Figure 2.2: SE SEM microstructure of, (a) as-received and (b) ball-milled $Ti_3SiC_2$.

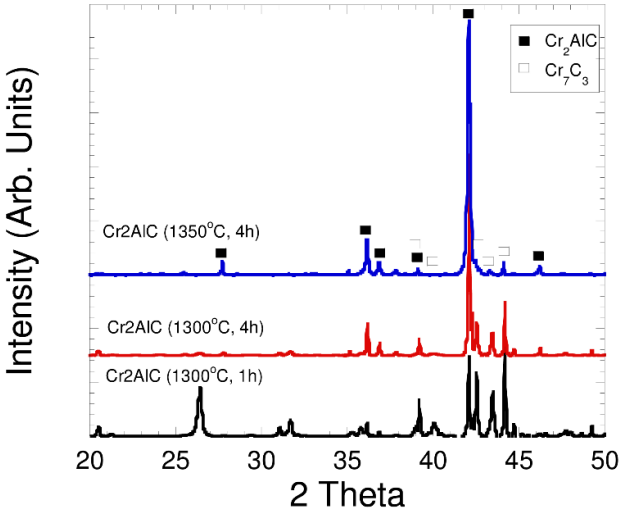


Figure 2.3: Plot of XRD of Composition B fabricated at, (a) 1300 ºC for 1 h, (b) 1300 ºC for 4 h, and (c) 1350 ºC for 4 h.

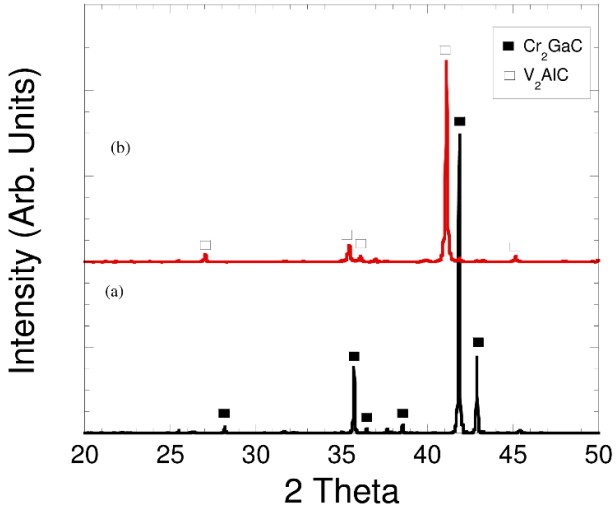


Figure 2.4: Plot of XRD of, (a) Composition C after heat treatment at 1100 ºC for 180 min, and (d) Composition D after heat treatment at 1550 ºC for 120 min.

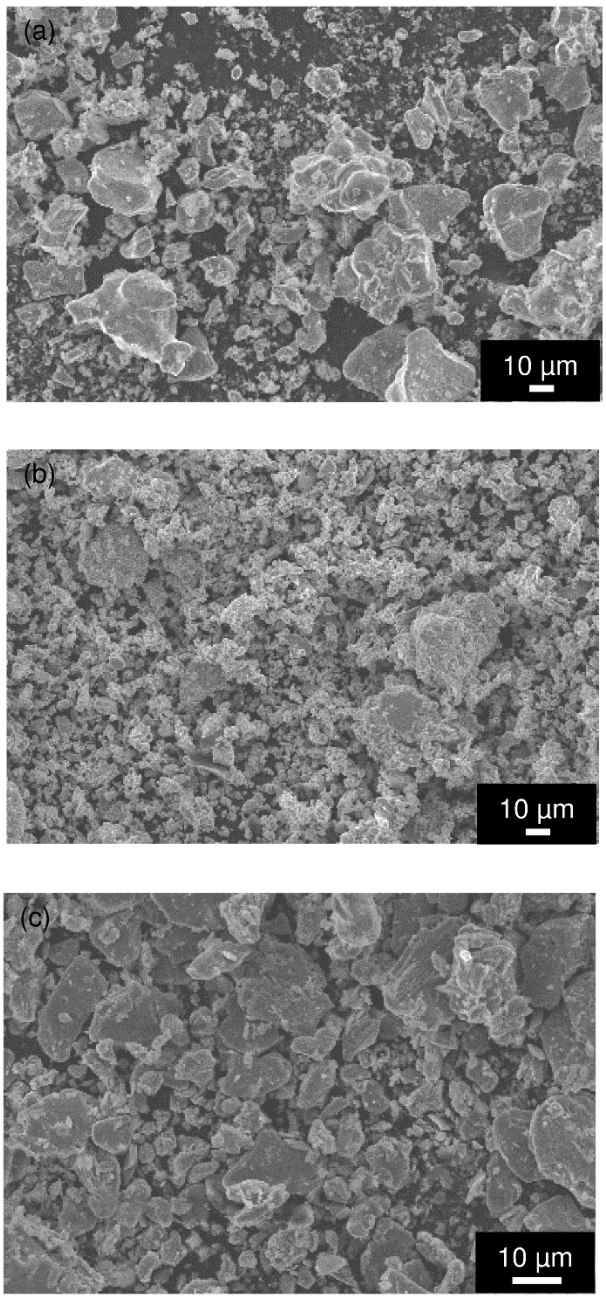


Figure 2.5: SE SEM micrographs of synthesized powders of, (a) $Cr_2AlC$, (b) $Cr_2GaC$, and (c) $V_2AlC$.

Xue et al. [14] and Su et al. [15] had also reported the synthesis of $Cr_2AlC$ particulates within a similar temperature range. Similarly, Figure 2.4 shows the XRD patterns of $Cr_2GaC$ (Composition C) and $V_2AlC$ (Composition D) powders after heat treatment at 1100 $^oC$ for 200 min

and 1550 $^{o}$C for 120 min, respectively. Both the compositions showed the formation of single phase of $Cr_2GaC$ and $V_2AlC$, respectively. Earlier, Cuskelly et al. [16] have reported the synthesis of $Cr_2GaC$ by carbothermal process. This is the first report to synthesize $Cr_2GaC$ particulates by sintering. Earlier, Neguib et al. [17] have reported the synthesis of $V_2AlC$ particulates by sintering at 1500 $^{o}$C for 4h. Figure 5 shows the typical distribution of the ball milled and sieved particles of different compositions. In future, these particulates can be used for designing composites.

**2.4 Conclusions**

The important conclusions of this paper are: (a) the particle size of $Ti_3SiC_2$ particulates can engineered by ball milling, (b) $Cr_2AlC$ particulates can be synthesized after sintering at 1350 $^{o}$C for 4 h, (c) $Cr_2GaC$ particulates can be synthesized by sintering at 1100 $^{o}$C for 200 min, and (d) $V_2AlC$ particulates can be synthesized after sintering at 1550 $^{o}$C for 120 minutes.

# CHAPTER III

# SYNTHESIS OF MoAlB PARTICULATES AND THEIR POROUS DERIVATIVES BY SELECTIVE DEINTERCALATION OF Al FROM MoAlB

This work was published in the proceedings titled Energy Technology 2018: Advanced Materials for Energy Conversion and Storage, "Synthesis of MoAlB Particulates and Their Porous Derivatives by Selective Deintercalation of Al from MoAlB", S. Gupta, M. Fuka., TMS 2018, DOI: https://doi.org/10.1007/978-3-319-72362-4_50.

## 3.1 Introduction

By now, it is well established that 2D materials have unusual electronic, mechanical, and optical properties which have led to their extensive study in the past decade for diverse applications [1-9]. Several types of novel 2D materials, for example, single-element 2D materials like graphene [1-3], silicone [4], germanene [5], and phosphorene [6]; two elements like dichalcogenides and oxides or more elements like clays [3, 7, 8] have been studied. For further tuning the properties, it is critical to design novel chemistries where these complex layers can contain more than one element which can offer novel properties as they provide different compositional variable for tuning the specific properties [9, 10].

MXenes are a promising addition to the novel 2D materials as they can be synthesized in different types of chemistry [9, 10]. More particularly, MXenes can be fabricated by selective

etching of A group element from MAX phases [9, 10]. As a background, $M_{n+1}AX_n$ (MAX) phases (over 70+ phases), where n =1,2,3; M is an Early Transitional Metal, A is a Group A element (mostly groups 13 and 14); and X is C and/or N, are novel ternary carbides and nitrides (space group *P6₃/mmc*) [11-14]. In these solids, the selective etching of A-element from the layers are possible as the M–A bonds are more chemically active than the stronger M–X bonds [9]. Neguib et al. [10] reported for the first time that 2D nanosheets, composed of a few $Ti_3C_2$ layers and conical scrolls, can be produced by exfoliating $Ti_3AlC_2$ in hydrofluoric acid. Later, Ghidiu et al. [15] demonstrated that MXene can be synthesized by etching in HCl–LiF solution where HCl and LiF react to form HF *in situ*, which then selectively etches the A atom from MAX phases. MXenes have also been derived from non-MAX-phase precursors, for example, $Mo_2CT_x$ is fabricated by etching Ga layers from $Mo_2Ga_2C$ [16]. These fundamental research has showed that 2D solids can potentially derived from complex ternary phases.

Ternary transition metal borides where boride sub-lattice is interleaved by one or two Al layers in $M_2AlB_2$-type (space group *Cmmm*) and MAlB-type (space group *Cmcm*) are promising candidates for exfoliation because of above mentioned reasons [17, 18]. Ade et al. [19] noted the similarity of these phases to MAX Phases and referred to these ternary solids as “MAB-phases”. In a recent paper, Kota el al. [20] reported dense and predominantly single-phase MoAlB by using a reactive hot pressing method. In this proceeding paper, we will present a preliminary study to explore the etching behavior of MoAlB particulates.

### 3.2 Experimental

Initially, MoAlB powder was fabricated by mixing powders of MoB (Part number 12563 (99% pure), Alfa Aesar, Haverhill, MA) and Al powder (Part number 11067 (99.5% pure), Alfa Aesar, Haverhill, MA) in the molar ratio of 1:1.2 by dry ball milling (8000 M mixer Mill, SPEX

SamplePrep, Metuchen, NJ) for 5 minutes. Thereafter, the powders were cold pressed, and annealed at 750 $^{o}$C for 2h at a ramp rate of 10 $^{o}$C/min. The annealed samples were then heat treated at a ramp rate of 10 $^{o}$C/min to 1550 $^{o}$C for 120 min in a tube furnace under flowing Ar. XRD analysis was performed to confirm whether the reacted powders were single phase (Fig. 3.1a). Predominantly single phase MoAlB powder was then ball milled and sieved until -325 mesh by using a sieve shaker.

MoAlB particulates were etched by treating the particulates with ~40 ml of 12 M HCl (ACS reagent 37%, Sigma Aldrich, St. Louis, MO) and 1 g (~1 M) LiF (BioUltra, ≥99.0%, Sigma Aldrich, St. Louis, MO). Initially, 1 M LiF was dissolved in 40 ml of 12 M HCl by stirring in a glass container on a heated plated by Teflon coated magnetic stirrer at ~40 $^{o}$C for ~15 min. Thereafter, 1 g (~0.2 M) of MoAlB was added to the stirring solution. The resulting suspension was stirred for ~40 h at ~40 $^{o}$C. The resulting suspension was then centrifuged at ~3,000 rpm for 5 min. The resulting filtrate was drained, and fresh DI (distilled) water was added to the residue. The suspension was centrifuged again for 5 min. This cycle was continued for 6 cycles until the pH was 6. The resulting suspension was sonicated. Few drops were collected for microscopy analysis and rest of the suspension was then dried in oven at ~100 $^{o}$C. XRD analysis was then performed on the dried and etched particulates. In the future, the authors plan to perform centrifugation after the sonication step to compare the results with current study.

Rigaku Diffractometer (SmartLab, Rigaku, Japan) was used for all XRD measurements at a step size of 0.02 $^{o}$ and scan rate of 4 $^{o}$/min from 20$^{o}$ to 70$^{o}$. JEOL JSM-6490LV Scanning Electron Microscope (JEOL USA, Inc., Peabody, Massachusetts.) was used to obtain Secondary electron (SE) and Backscattered Electrons (BSE) images of the synthesized MoAlB particulates. X-ray information was obtained via a Thermo Nanotrace Energy Dispersive X-ray detector with NSS-

300e acquisition engine. All the other images were taken by Field Emission Scanning Electron Microscope (FESEM) in SE (Secondary) and BSE (Backscattered Electron) mode by a JEOL JSM-7600F scanning electron microscope (JEOL USA, Inc., Peabody, MA). Energy-dispersive spectroscopy information was acquired by using an UltraDry silicon drift X-ray detector and NSS-212e NORAN System 7 X-ray Microanalysis System (Thermo Fisher Scientific, Madison, Wisconsin.).

For qualitative comparison, the length (l) and width (w) of pores in the etched grain was measured by Image J software [21]. An average of 10 pores are reported for a sample.

### 3.3 Results and Discussion

XRD pattern shows that MoAlB is the predominant phase in the pattern (Fig. 3.1). Figure 3.2 shows the morphology of MoAlB particulates. However, at higher magnification, micron sized $Al_2O_3$ particles were also detected. Based on the XRD and SEM results (Figs. 3.1 and 3.2), it can construed that the MoAlB formed during the synthesis process is predominantly single phase (Fig. 2b).

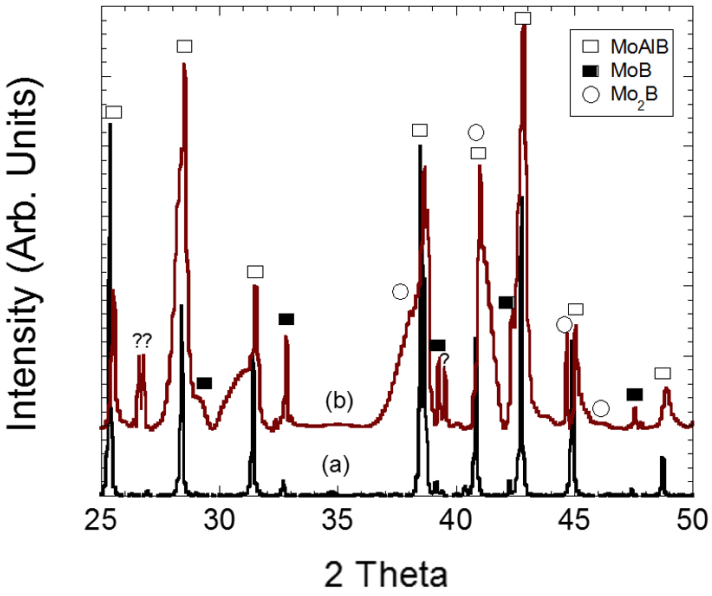


Figure 3.1: XRD plot of, (a) MoAlB, and (b) etched MoAlB particulates.

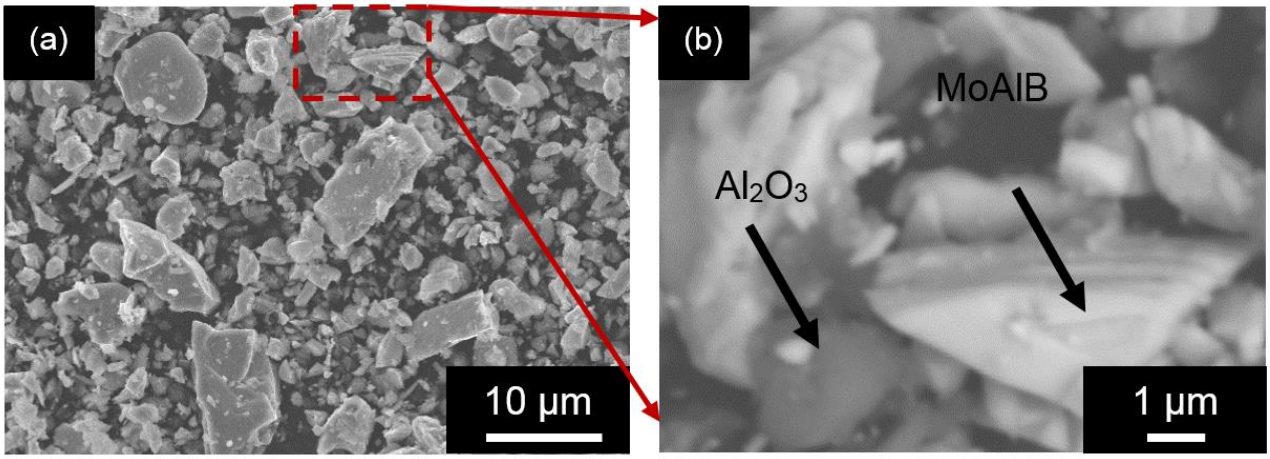


Figure 3.2: SEM SE micrograph of as-synthesized MoAlB particulates at, (a) lower, and (b) BSE image at higher magnifications.

Figure 3.3 shows the morphology of different particulates after the chemical treatment. Figure 3.3a shows an overview of etched surface of different particulates. Several particulates are observed with etched surfaces. On a closer inspection of the top surface of a single particulate (Fig. 3.3b-d), it seemed that several interconnected 2D layers within a single particulate are present. In addition, the pores between the layers are linear and highly anisotropic, for example, on average - the length of the interlaminar pores was 257±126 nm, and the width of the pores was 35±10 nm. The EDS analysis of the particulate showed the composition of a region is $(Mo_{0.67}Al_{0.33})B\{O_{0.19}F_{0.02}\}$. The reaction of HCl and LiF resulted in the in situ formation of HF [16]. The HF formed by in situ reaction reacts with the MoAlB particulates, and the Al is then selectively etched from the particulates. XRD of the etched MoAlB particulates showed that the MoAlB peaks are broadened as compared to the as-synthesized MoAlB which further support the formation of Al-deficient MoAlB (Fig. 3.1). Figures 3.3e-f shows the morphology of edge of an etched particulate. Several pores (< 100 nm) were observed on the surface. Detailed TEM studies are needed to document the crystal structure of these etched phases. The XRD pattern also detected

the presence of $Mo_2B$ and MoB which indicate that some of the particulates have converted fully to binary borides. Based on the oxidation results, Kota et al. [20] also reported that MoAlB can exist with a deficiency of Al, thus MoAlB phase can be a potential candidate for particulate design.

The chemistry of etched particulates ($(Mo_{0.67}Al_{0.33})B\{O_{0.19}F_{0.02}\}$) is very similar to MXenes which have a general formula of $M_{n+1}X_nT_x$, where T represents the surface terminations which is a combination of –OH, –O and –F groups [9]. This study shows that novel particulates can be designed by partial selective etching of Al from MoAlB (MAB Phases). The stacked layers are reminiscent of multilayered MXenes (Fig. 2 in Ref. 9), but the multilayers are connected in this case (Fig. 3.3d). Due to structural similarity to multilayered MXenes, these novel particulates

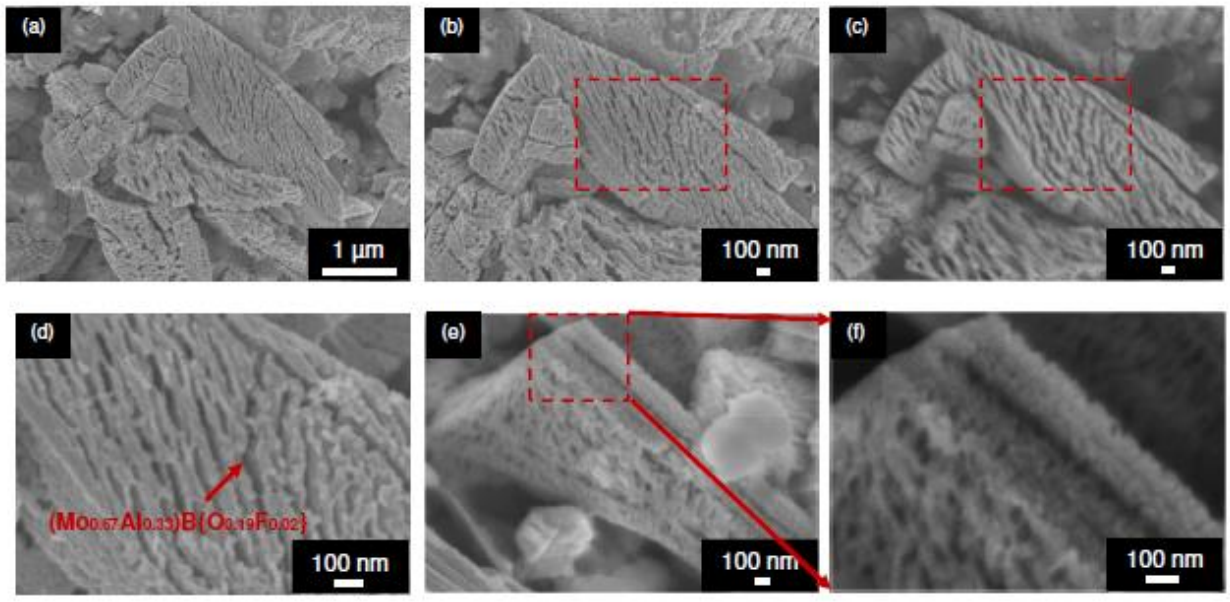


Figure 3.3: FESEM SE micrographs of, (a) etched MoAlB particulates, (b) top surface of etched MoAlB particulate at higher magnification, (c) BSE of the same region, (d) higher magnification of the marked region in (b), (e) side view of an etched particulate, and (f) higher magnification of the same region.

can be referred as MABenes as the Al is not completely deintercalated from the MoAlB particulate. Authors accept the fact that more detailed studies are needed to understand the

composition of filtrate as it may possible that residual $AlF_3$ is trapped inside the porous structures. As mentioned the experiment section, the authors plan to perform centrifugation after the sonication step to compare the results with current study. In an excellent review article, Anasori et al. [9] summarized that etching rate of Al-containing MAX phases is dependent on the atomic number of M, for example M with larger atomic number requires a longer and stronger etching. In addition, MXenes with larger *n* in $M_{n+1}C_nT_x$ require stronger etching and/or a longer etching time. For example, $Mo_2Ti_2AlC_3$ ($n$ = 3) requires an etching time that is twice as long as its $n$ = 2 counterpart (that is, $Mo_2TiAlC_2$) under the same etching conditions [9]. Based on these findings, it can be further hypothesized that by optimizing the etching conditions, it will be possible to generate MXene like MBene phases which will offer scientists more flexibility in materials design for energy applications.

Interestingly, there has not been significant study on the design of particulates by partial etching of MAX phases. It is also hypothesized that MAXenes particulates can be fabricated by the partial etching of MAX Phases.

### 3.4 Conclusions

Novel porous particulates were designed by deintercalation of MoAlB particulates by treating them with a solution of LiF and HCl. These particulates showed a unique stacked 2D-particles like morphology and were riddled with pores of dimensions 257±126 nm and 35±10 nm, respectively. The EDS analysis showed that particulates had a chemistry of $(Mo_{0.67}Al_{0.33})B\{O_{0.19}F_{0.02}\}$ due to partial deintercalation of Al from MoAlB.

# CHAPTER IV

# NOVEL TERNARY BORIDE (MoAlB) PARTICULATES AS SOLID LUBRICANT ADDITIVES IN NI-MATRIX COMPOSITES

This work has been accepted for publication in 2018 Joint Propulsion Conference, AIAA Propulsion and Energy Forum and Exposition, Additive Manufacturing for Propulsion Systems II Session, "Novel Ternary Boride (MoAlB) Particulates as Solid Lubricant Additives in Ni-Matrix Composites", M. Fuka, M. Dey, S. Gupta, AIAA, 2018.

## 4.1 Introduction

$M_{n+1}AX_n$ (MAX) phases, where n =1,2,3; M is an Early Transitional Metal, A is a Group A element (mostly groups 13 and 14); and X is C and/or N, are novel ternary carbides and nitrides (space group $P6_3/mmc$) which have attracted a lot of attention due their excellent properties like damage tolerance, thermal shock resistance and machinability [1-4]. Although MAX Phases exist in a range of chemistry but there is no MAX phase where X = B. Jeitschko et al. [5, 6] had reported the $M_2AlB_2$-type (space group *Cmmm*) and MAlB-type (space group *Cmcm*) ternary transition metal borides where boride sub-lattice is interleaved by one or two Al layers, respectively. Okada et al. [7] had reported the synthesis and characterization of single crystals of MoAlB, WAlB, $(Mo_xCr_{1-x})AlB$, and $(Mo_xW_{1-x})AlB$ by the flux method by using molten aluminum as a solvent. Ade et al. [8] had also successfully synthesized single crystals of $Cr_2AlB_2(CrB_2)_x$ (x = 0, 1, 2), $M_2AlB_2$ (M = Cr, Mn, Fe), and MAlB (M = Mo, W). The authors noted the similarity to MAX Phases and classified these ternary solids as "MAB-phases". Recently, Kota et al. [9] reported

dense and predominantly single-phase MoAlB by using a reactive hot pressing method. They also confirmed that by High-resolution scanning transmission electron microscopy that indeed two Al layers is present between a Mo-B sublattice. More importantly, unlike the binary transition metal borides, MoAlB followed cubic time-dependent oxidation kinetics and formed a dense alumina scale when heated in air. In addition, MoAlB showed metal like characteristics where resistivity drops linearly with decreasing temperatures accompanied with a low resistivity of (0.36–0.49 μΩm) at RT. It was also reported that MoAlB is a good thermal conductor (35 $Wm^{-1}K^{-1}$ at 26 °C). High temperature studies also indicated that the compound is stable to at least 1400 °C in inert atmospheres and has moderately low Vickers hardness values of (10.6 ± 0.3) GPa (Okada et al. [7] reported a hardness of ~10.3 GPa), compared to other transition metal borides, and ultimate compressive strengths of 1940 ± 103 MPa at room temperature. The authors also proposed that these encouraging results warrant further study of this compound for potential usage at higher temperatures.

Recently, Gupta et al. [10-13] showed that the addition of MAX phase ($Ti_3SiC_2$) particulates enhanced the mechanical and tribological performance of Al-, Zn-, Bi- Ag- and Ni-matrix composites. The authors had referred to these new generation of composites as MRM (Metal Reinforced with MAX) as 5-30 vol% $Ti_3SiC_2$ was used to reinforce the metal matrix. In this paper, we will report the effect of MoAlB particulates on the mechanical and tribological behavior of Ni-based composites. These composites will be referred to as MRMB (Metals Reinforced with MAB).

**4.2 Experimental**

Initially, MoAlB powder was fabricated by mixing powders of MoB (Part number 12563 (99% pure), Alfa Aesar, Haverhill, MA) and Al (Part number 11067 (99.5% pure), Alfa Aesar,

Haverhill, MA) in the molar ratio of 1:1.2 by dry ball milling (8000 M mixer Mill, SPEX SamplePrep, Metuchen, NJ) for 5 minutes. Thereafter, the powders were cold pressed, and annealed at 750 °C for 2h at a ramp rate of 10 °C /min. The annealed samples were then heat treated at a ramp rate of 5 °C/min to 1000, 1250, and 1550 °C for 120 min in a tube furnace under flowing Ar. XRD analysis was performed to confirm whether the reacted powders were single phase (detailed discussion in next section). Predominantly single phase MoAlB powder was then ball milled and sieved until -325 mesh by using a sieve shaker. Novel Ni-based composites were then designed by adding 5 vol% (Ni-5%MoAlB), 10 vol% (Ni-10%MoAlB), 20 vol% (Ni-20%MoAlB), and 30 vol% (Ni-30%MoAlB) MoAlB in the Ni- matrix by hot pressing. Initially, the phase pure MoAlB particulates was mixed with the desired amount of Ni powders (Part number 43214 (-325 mesh and 99.8% pure), Alfa Aesar, Haverhill, MA) by dry ball milling for 5 minutes. The powders were then cold pressed under a uniaxial compressive stress of ~88 MPa (~12.7 mm die), and then hot pressed (HP) under a uniaxial compressive stress of ~240 MPa with the same die at 600 °C for 5 minutes. For comparison, samples of pure Ni were also fabricated by following the above-mentioned procedure. In addition, Ni-MoAlB composites were also cold pressed at ~88 MPa and then hot pressed at 600 °C for 5 minutes by using a compaction pressure of ~165 MPa by using MoAlB powders synthesized at 1550 °C. In this paper, following nomenclature will be used to designate samples: Ni-vol%MoAlB (temperature)(pressure), for example, Ni-30%MoAlB(1550 °C)(240 MPa) means that Ni matrix composite was reinforced with 30 vol% MoAlB (precursor MoAlB powders were synthesized at 1550 °C) by hot pressing the ball milled composition at 240 MPa at 600 °C for 5 minutes.

Relative density was determined by dividing the experimental density with theoretical density. The experimental density of the composites was measured from the mass and dimensions

of each sample. Rule of mixture was used to calculate the theoretical density of all the composite samples by using the nominal composition, theoretical density of MoAlB and Ni particulates. The compositions were machined by a diamond saw into ~3 mm cubes for mechanical testing. All the samples were then tested in compression by using a mechanical testing unit (Shimadzu AD-IS UTM, Shimadzu Scientific Instruments Inc., Columbia, MD) at a deflection rate of 1 mm/min. For each composition, a set of 5 samples were tested. Stress versus displacement plots are reported as experimental limitations did not allow for accurate measurement of the actual strain during mechanical testing. In this paper, the yield strength is defined as the critical stress at which the stress verse displacement plot transitions from the linear to non-linear regime, and the linear region of the plot had a regression fitting of $R^2 > 0.95$. For each composition, an average of 5 yield strength measurements is reported in the text [10-13]. All composites were polished ($R_a < 1$ μm) and then tested by a Vicker's micro-hardness indentor (Mitutoyo HM-112, Mitutoyo Corporation, Aurora, IL) at 4.9 N for 12 s.

Rigaku Diffractometer (SmartLab, Rigaku, Japan) was used for all XRD measurements at a step size of 0.02 $^o$ and scan rate of 4 $^o$/min from 20$^o$ to 50$^o$. The tribological behavior of the hot pressed and polished disc shaped samples (every sample has a surface roughness of $R_a$ <1 μm determined by using a surface profilometer (Surfcom 480A, Tokyo Seimitsu Co. Ltd., Japan)) were tested by using a ball-on-disc tribometer (CSM Instruments SA, Peseux, Switzerland) at 5 N, 31.4 cm/s linear speed, ~5 mm track radius, and a sliding distance of 200 m while sliding against stainless steel (SS) (100Cr6 (~6 mm diameter), Anton Paar USA Inc., Ashland, VA) and alumina (Anton Paar USA Inc., Ashland, VA) balls. For each composition, a set of 3 measurements were performed, and the mean of the individual average reading from the three data set was calculated and reported in the text as $\mu_{mean}$. During tribological testing, the mass of the samples and substrates

were measured before and after the experiments by using a weighing scale (Model XA82/220/2X, Radwag Balances and Scales, Poland). The specific wear rate (WR) was calculated from:

$$WR = (m_i - m_f)/(\rho.N.d) \quad \text{----------(I)}$$

where, $m_i$ is the initial mass, $m_f$ is the final mass, $\rho$ is density of the composite, N is the applied load, and d is the total distance traversed by the tab during the tribology testing [10-13].

All the samples were characterized by JEOL JSM-6490LV Scanning Electron Microscope (JEOL USA, Inc., Peabody, Massachusetts.) in Secondary electron (SE) and Backscattered Electrons (BSE) mode. X-ray information was obtained via a Thermo Nanotrace Energy Dispersive X-ray detector with NSS-300e acquisition engine. The accuracy of measuring C and B is quite low during chemistry analysis by X-ray detector in SEM. It is also possible that some of the compositions listed, for example sub-stoichimetric oxides and other phases, may contain C and/or B which is very difficult to determine experimentally. Thus, a combination of BSE and X-ray analysis is used to determine the tribochemistry of tribocouples. If a region is determined to be chemically uniform then it will identified with two asterisks as *microconstituent* to emphasize that these areas are not necessarily single phases. Please note, it is a qualitative methodology to compare the tribochemistry of different *microconstituents*. Furthermore, the presence of C and/or B in these tribofilms will be shown by adding $\{C_x\}$ or $\{B_y\}$ in the microconstituent [10-13].

### 4.3 Results and Discussion

#### 4.3.1 Microstructure and Phase Analysis

Figure 4.1 shows the morphology of powders fabricated at different temperatures. In all cases, the powders were speckled with Al-rich oxides. It is not clear, what is causing the formation of these oxides. In addition, EDS results also showed that MoAlB phases have some O solubility.

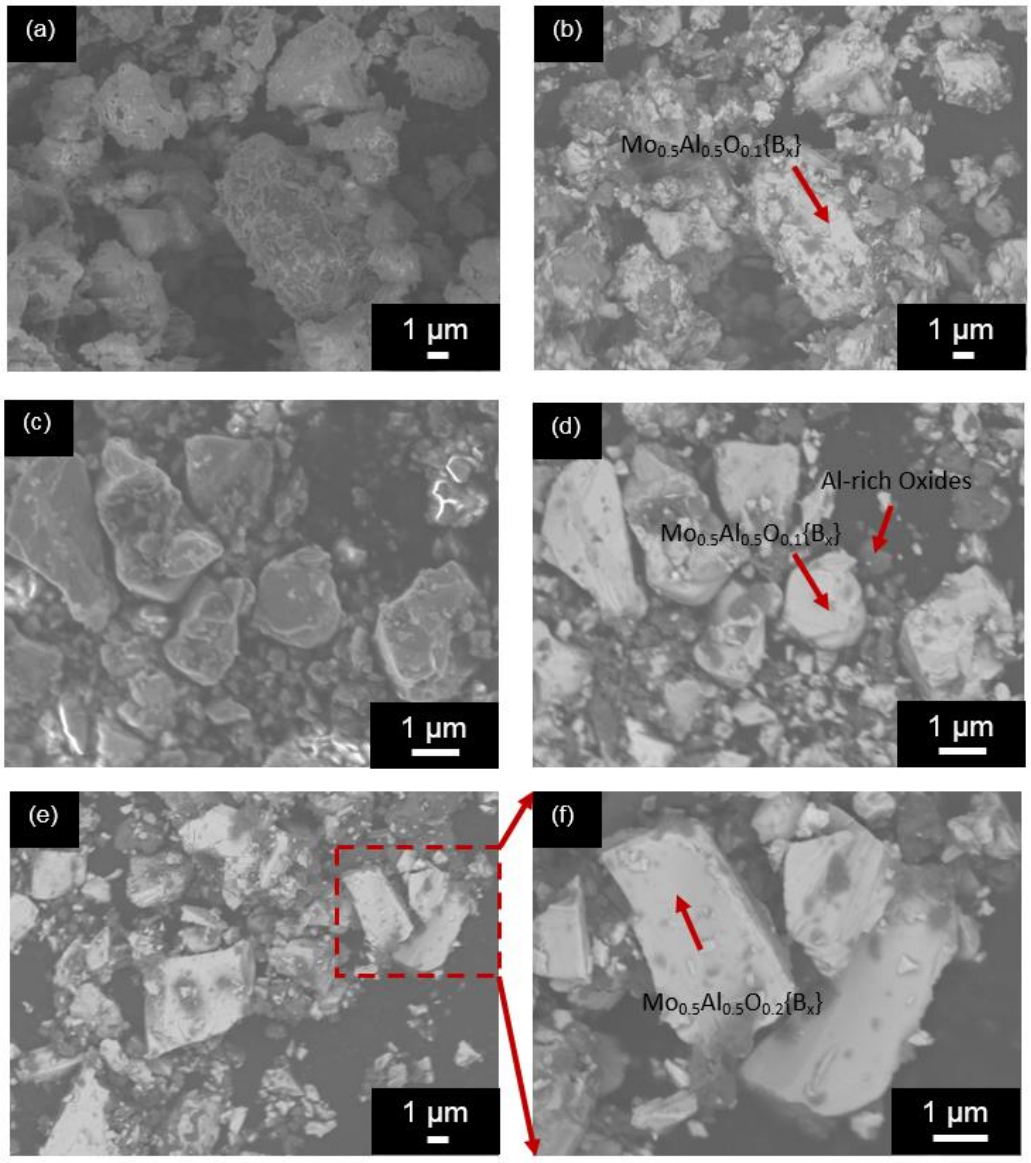


Figure 4.1: FESEM micrographs of MoAlB particles synthesized at, (a) 1000 $^{o}$C in SE, (b) BSE of the same region, (c) 1250 $^{o}$C in SE, (d) BSE of the same region, (e) 1550 $^{o}$C in BSE, and (f) BSE at higher magnification.

Figure 4.2a also confirmed that the powders synthesized at different temperatures were predominantly single phase, but the concentration of residual MoB increased as the synthesis temperature was increased from 1000 to 1550 °C. This fact should be further explored in future studies. Figure 4.2b shows the XRD pattern of Ni-MoAlB composites where predominantly MoAlB and Ni peaks were detected.

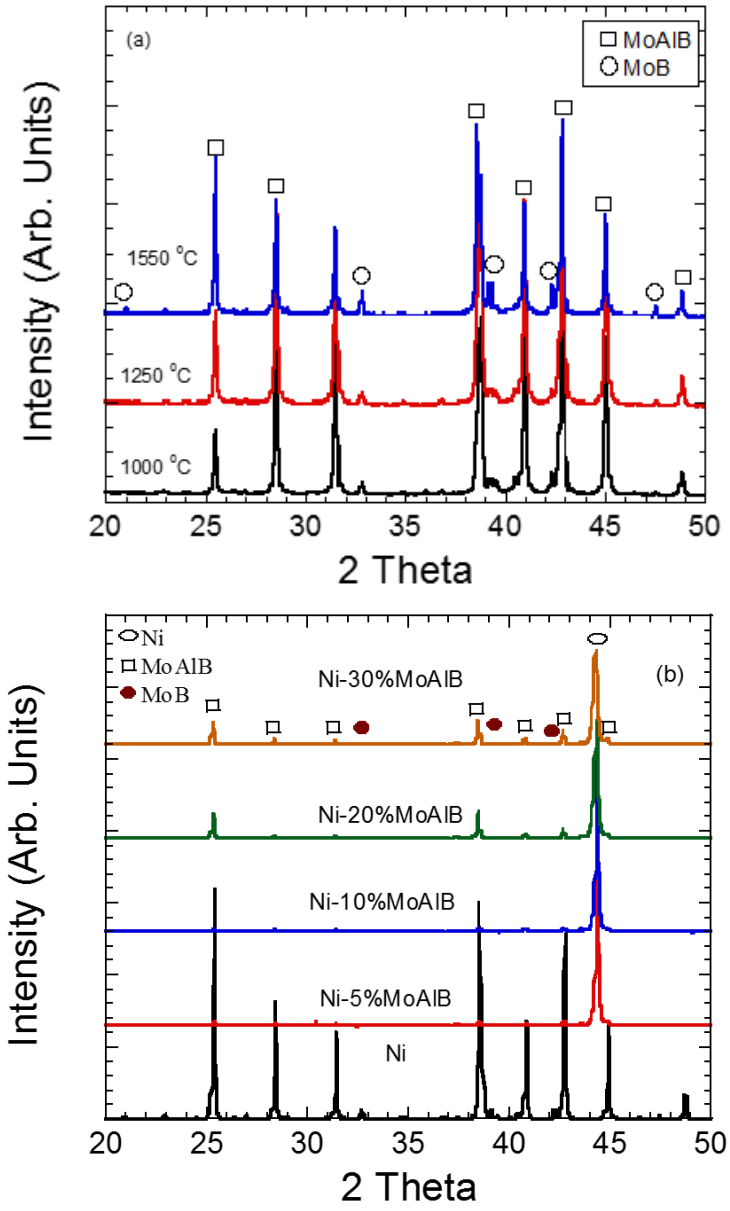


Figure 4.2: XRD plots of, (a) MoAlB powders synthesized at different temperatures, and (b) Ni-MoAlB composites fabricated at 1550 °C and 240 MPa.

Figure 4.3 summarizes the SEM micrographs of Ni-MoAlB composites. In all the micrographs, MoAlB particles were nestled inside the Ni-matrix with minimal or negligible interfacial reactions. For example, the inset of Fig. 4.3e shows the higher magnification of MoAlB particle embedded inside the Ni-matrix where minor interfacial reaction resulted in the formation of a Ni-rich dark phase ($Mo_{0.2}Al_{0.3}Ni_{0.5}O_{0.3}\{B_x\}$) at the corner of the MoAlB particulate.

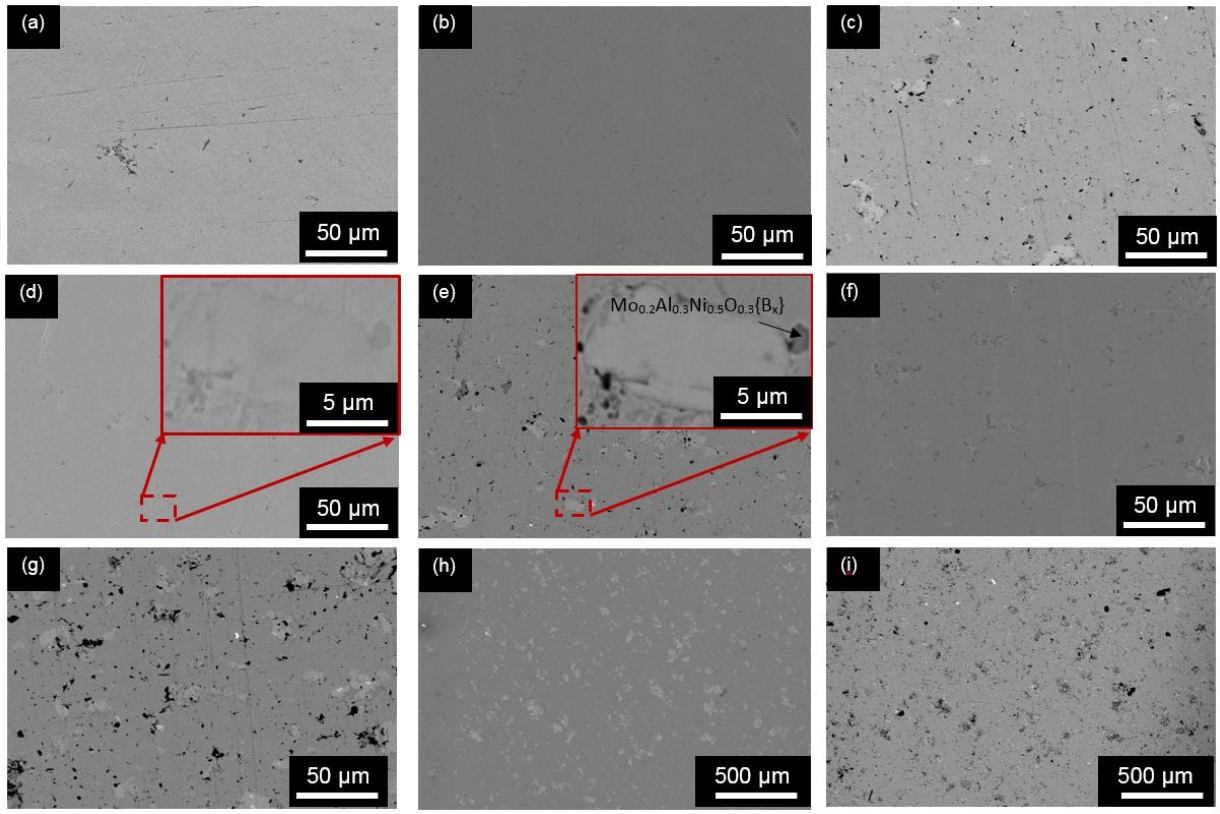


Figure 4.3: SEM micrographs of, (a) Ni in SE, (b) Ni-5%MoAlB (1550 °C)(240 MPa) (SE), (c) BSE of the same region, (d) Ni-10%MoAlB (1550 °C)(240 MPa) in SE, (e) BSE image of the same region (inset shows the high magnification of the interface), (f) Ni-20%MoAlB (1550 °C)(240 MPa) in SE, (g) BSE of the same region, (h) Ni-30%MoAlB (1550 °C)(240 MPa) in SE, and (i) BSE image of the same region.

Figures 4.4a and 4.4b show porosity and hardness of the composites as a function of MoAlB additions, respectively. In all the samples, the addition of higher vol% of MoAlB increased the porosity. This study shows that it is difficult to densify these samples as the amount of MoAlB is increased in the metal matrix. Similar trend was also observed during the processing of Al [10], Zn [11], Ag [12], Bi [12], and Ni [13] based MRM composites. In addition, the samples fabricated at lower compaction pressure (165 MPa) showed high porosity as compared to samples fabricated at 240 MPa. The hardness increased from ~1.58 GPa in Ni (240 MPa) (porosity: ~10%) to ~1.43 GPa in Ni-10%MoAlB (1550 °C) (240 MPa) (porosity: ~17%), and retained similar value of ~1.37 GPa in Ni-30%MoAlB (1550 °C) (240 MPa) (porosity: ~24%). Comparatively, Ni (165 MPa) has a hardness of ~1.08 GPa (porosity: ~18%), it dropped gradually to 0.70 GPa in Ni-10%MoAlB (1550 °C) (165 MPa), but increased to 1.04 GPa in Ni-30%MoAlB (1550 °C) (165 MPa) although the samples had similar porosity of ~25%.

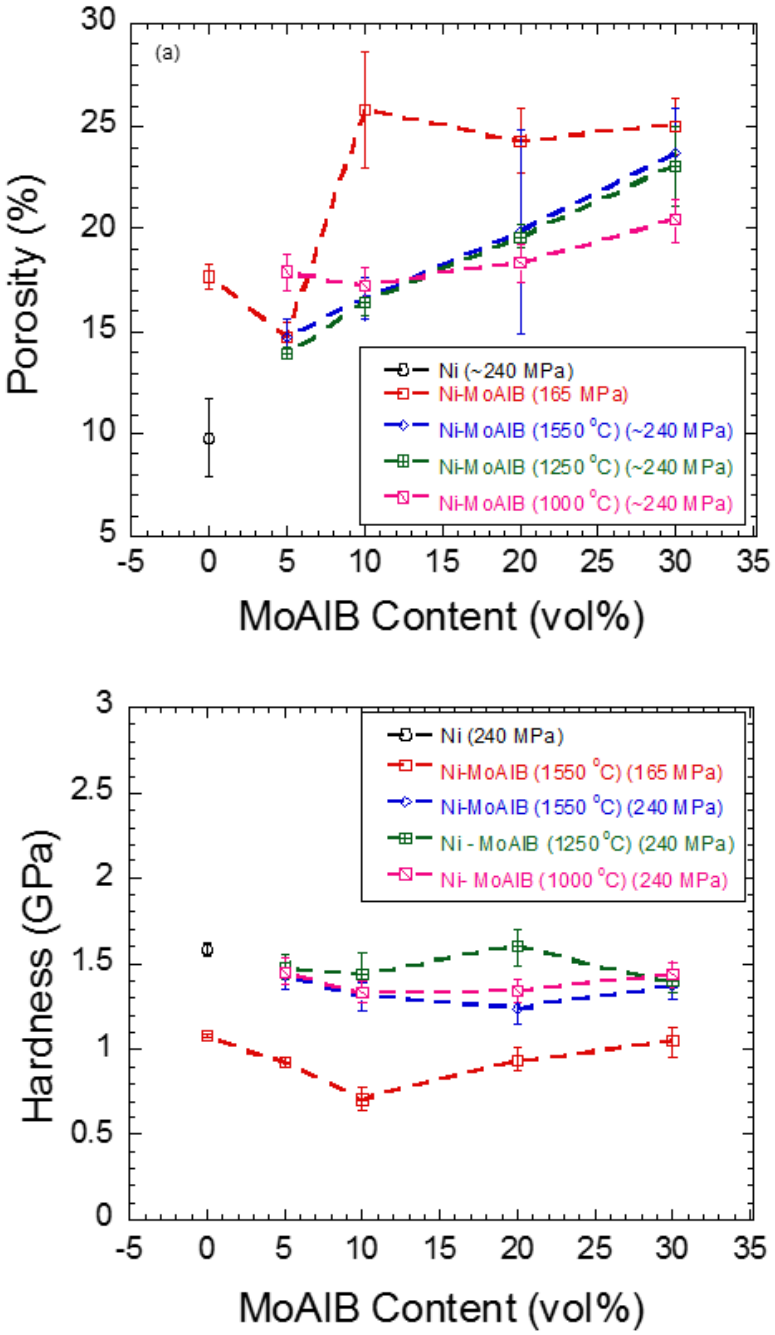


Figure 4.4: Plot of, (a) porosity, and (b) hardness versus MoAlB content in Ni-matrix.

Clearly, due to the presence of MAX phases, the Ni-matrix is able to retain similar hardness although the samples are becoming more porous. In a recent paper, we showed similar behavior in Ni-$Ti_3SiC_2$ composites [13]. These studies showed that hot pressing Ni-MoAlB or related

composites at lower temperature is a critical path for fabricating these composites. As far as authors are aware, this is the first study to report composites of Ni with MAB by powder metallurgy route. Earlier, Lia et al. [14] had reported poor wettability of Ni and $Ti_3SiC_2$ which resulted in reaction at the interfaces of Ni and $Ti_3SiC_2$ while sintering at 1450 °C for 90 min.

### 4.3.2 Mechanical Performance

Figure 4.5a shows the stress versus displacement plots of different composites. Ni and Ni-5%MoAlB showed ductile and gradual failure, and the failure became more brittle as the concentration of MoAlB was increased in the Ni- matrix. Figure 4.5b summarizes the yield strength of these composites. Initially, by inspecting the data, it seems that the yield strength decreases as the concentration of MoAlB particulates are increased in the Ni-matrix. If we inspect the data carefully, then we can observe that the yield strength decreased from ~600 MPa in Ni (240 MPa) (porosity: ~10%) to ~498 MPa in Ni-10%MoAlB (1550 °C) (240 MPa) (porosity: ~17%), thereafter it increased gradually decreased to ~403 MPa in Ni-30%MoAlB (1550 °C) (240 MPa) (porosity: ~24%). Comparatively, Ni (165 MPa) (porosity: 18%) had a yield strength of ~467.5 MPa, and it decreased gradually to ~290 MPa in Ni-30%MoAlB (1550 °C) (165 MPa) (~25% porosity). By comparing the date for similar porosity of Ni (165 MPa) and Ni-10%MoAlB (1550 °C) (240 MPa) (porosity: ~17%), it can be concluded that MoAlB particulates are able improve the yield strength while decreasing the ductility of the samples. More studies are needed delineate the effect of porosity and MoAlB content on the mechanical performance of these composites.

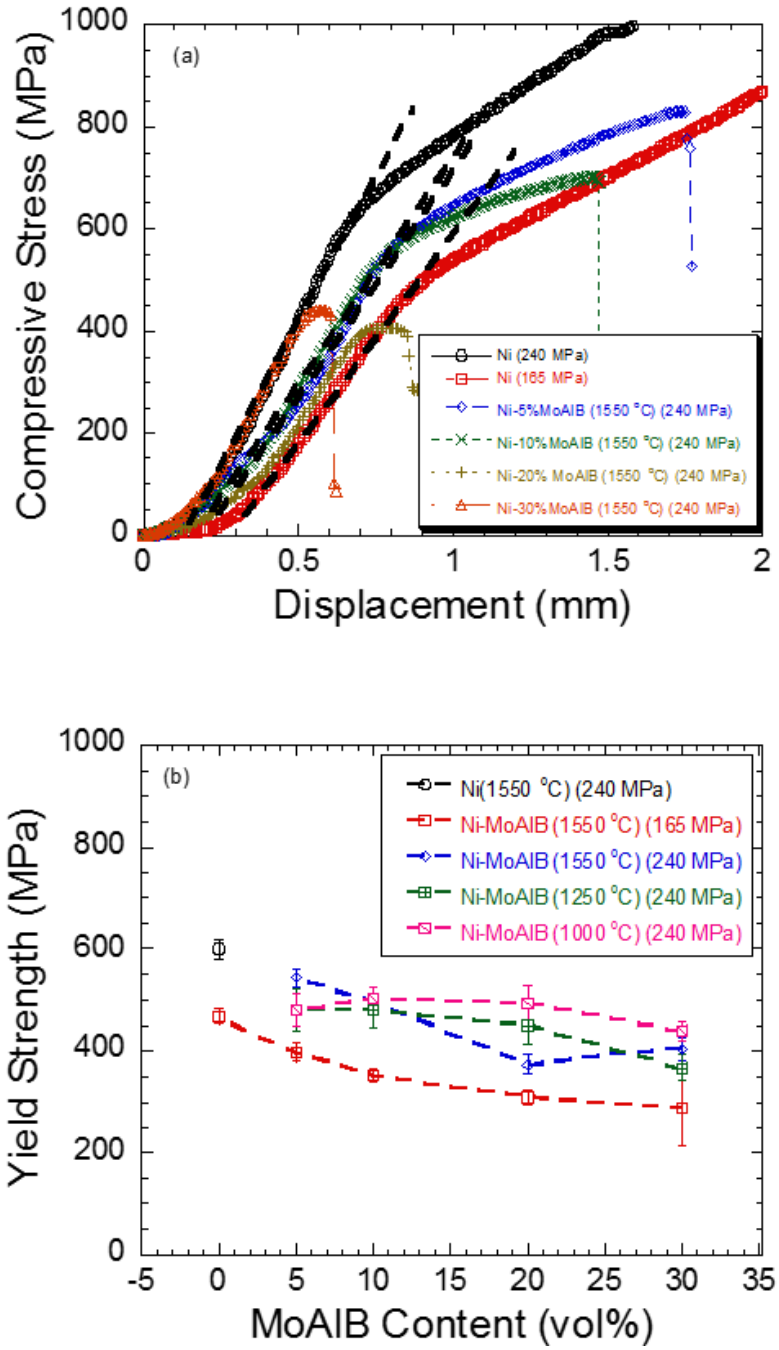


Figure 4.5: Plot of, (a) compressive stress versus displacement, and (b) yield strength versus MoAlB content.

### 4.3.3 Tribological Behavior of MRMBs

Figure 4.6a shows the plot of μ versus distance profile of Ni-MoAlB composites. In general, $\mu_{mean}$ increased as the concentration of MoAlB was increased in the Ni-matrix. For example in Ni-MoAlB composites and SS tribocouples, it increased gradually from ~0.55 in Ni to ~0.61 and ~0.70 in Ni-10%MoAlB (1550 °C) (240 MPa) and Ni-30%MoAlB (1550 °C) (240 MPa), respectively (Fig. 4.6a). Comparatively, in Ni-MoAlB composites and $Al_2O_3$ tribocouples, it increased from ~0.28 in Ni (240 MPa) to ~0.49 and ~0.66 in Ni-10%MoAlB (1550 °C) (240 MPa) and Ni-30%MoAlB (1550 °C) (240 MPa), respectively (Fig. 4.6b). On further comparison with Ni-$Ti_3SiC_2$ composites, it can be observed that these composites showed similar behavior as Ni-MoAlB composites, for example against SS, the $\mu_{mean}$ was ~0.78 and ~0.86 in Ni-10%$Ti_3SiC_2$ and Ni-30%$Ti_3SiC_2$, respectively. Similarly against alumina, $\mu_{mean}$ was ~0.54 and ~0.55 in Ni-10%$Ti_3SiC_2$ and Ni-30%$Ti_3SiC_2$, respectively.

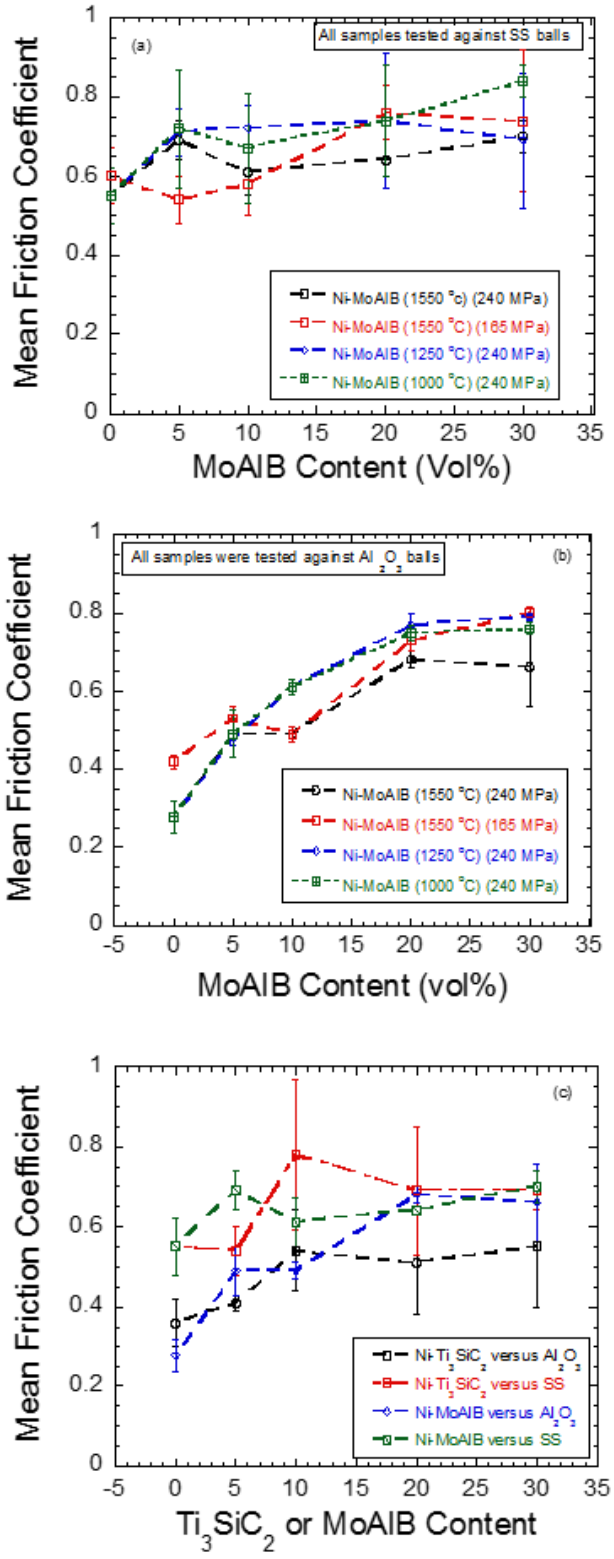


Figure 4.6: Plot of mean friction coefficient ($\mu_{mean}$) versus MoAlB content during sliding against, (a) SS, and (b) alumina balls, and (c) comparison of $\mu_{mean}$ of Ni-$Ti_3SiC_2$ [13] or Ni-MoAlB (1550 °C) against SS and $Al_2O_3$ balls, respectively.

Figure 4.7 summarizes the plot of WR versus MoAlB content in Ni-matrix composites. During sliding against SS (Fig. 4.7a), the WR decreased gradually with MoAlB content, for example, it decreased from 3 x $10^{-3}$ $mm^3$/Nm in Ni (240 MPa) to ~5 x $10^{-4}$ $mm^3$/Nm in Ni-30%MoAlB (1550 °C) (240 MPa), ~8 x $10^{-4}$ $mm^3$/Nm in Ni-30%MoAlB (1250 °C) (240 MPa) and ~2 x $10^{-4}$ $mm^3$/Nm in Ni-30%MoAlB (1000 °C) (240 MPa), respectively. Interestingly, during sliding against alumina (Fig. 4.7b), the WR increased steadily from ~2.8 x $10^{-5}$ $mm^3$/Nm in Ni to ~1.8 x $10^{-4}$ in Ni-30%MoAlB (1550 °C) (240 MPa). Similar behavior was observed in all the different derivatives of Ni-MoAlB composites. Comparatively in Ni-$Ti_3SiC_2$ composites during sliding against SS, the WR decreased to mildly 2 x $10^{-3}$ $mm^3$/Nm in Ni-30%$Ti_3SiC_2$ (Fig. 4.7c). Similar trend like Ni-MoAlB composites sliding against alumina was observed in Ni-$Ti_3SiC_2$ composites but the increase in WR was comparatively higher, for example, Ni-30%$Ti_3SiC_2$ composite had a WR of 8 x $10^{-4}$ $mm^3$/Nm. These studies showed that MoAlB performs marginally better than $Ti_3SiC_2$ particulates. Detailed studies are needed to further explore the efficacy of MoAlB as a solid lubricant.

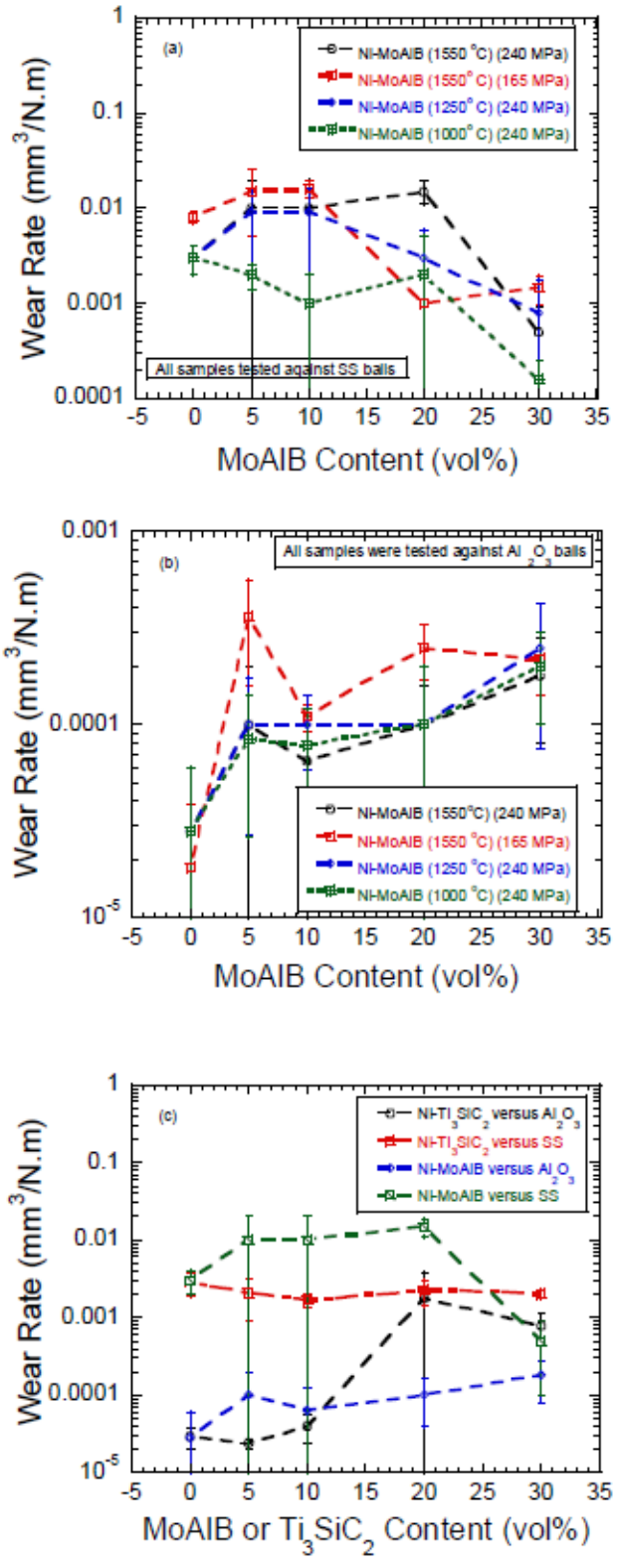


Figure 4.7: Plot of mean Wear Rate (WR) versus MoAlB content during sliding against, (a) SS, and (b) alumina balls, and (c) comparison of WR of Ni-$Ti_3SiC_2$ or Ni-MoAlB (1550 °C) after sliding against SS and $Al_2O_3$ balls, respectively.

Figures 4.8a-f show Ni and stainless surfaces after tribological testing. Signs of adhesive and oxidative wear was observed on both the tribosurfaces, for example, partially oxidized debris of * $Ni_{0.94}Fe_{0.06}O_{0.01}$* (Figs. 4.8a-b) and * $Ni_{0.98}Fe_{0.02}O_{0.40}$* (Figs. 4.8e-f) was observed on the Ni and stainless steel surface, respectively.

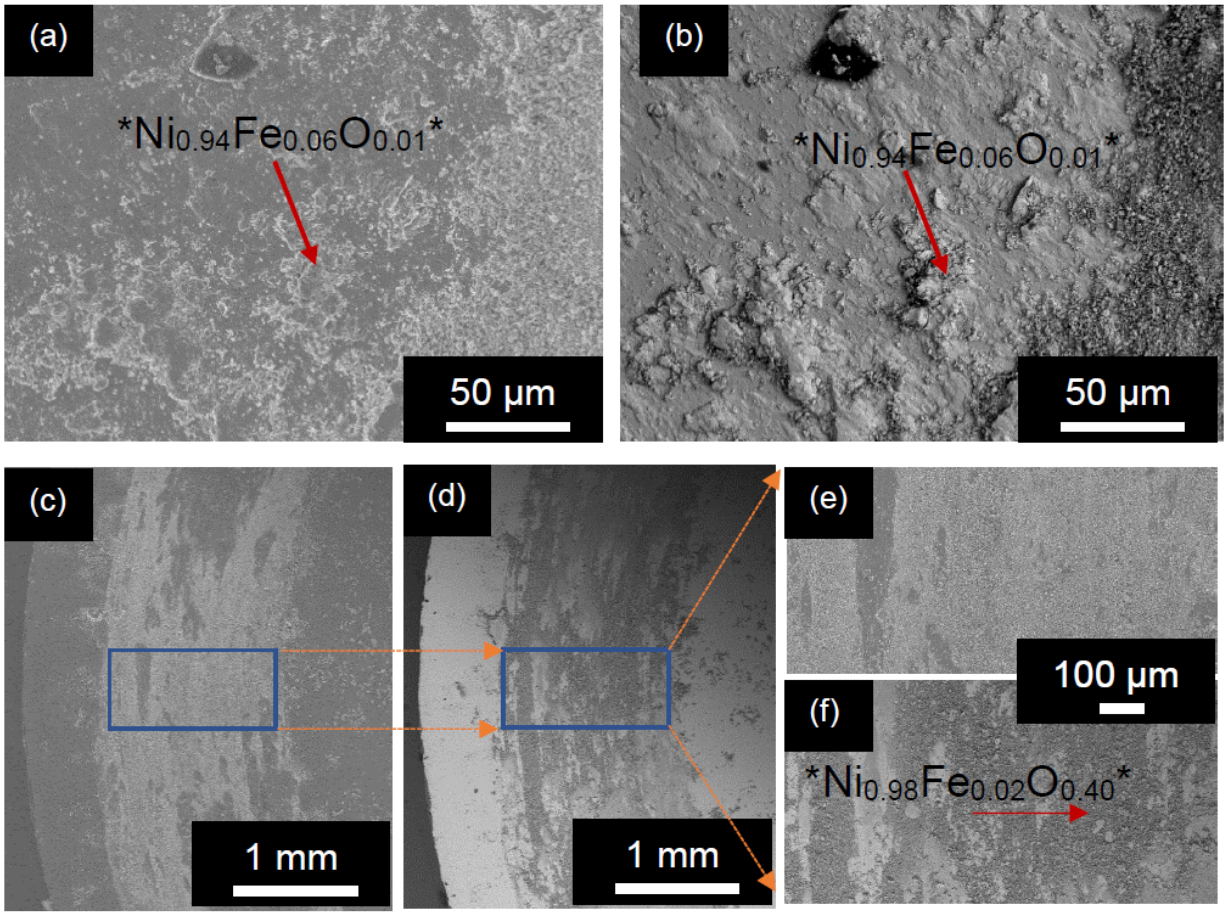


Figure 4.8: SEM micrographs of SS surface in, (a) SE, (b) BSE, and corresponding Ni surface in, (c) SE, (d) BSE, and higher magnification of the region marked in (d) in, (e) SE and (f) BSE during dry sliding.

Comparatively, Figs. 4.9a-b show SS surface and Figs. 4.9c-e show the Ni-30%MoAlB surface at lower (Figs. 4.9c-d) and higher magnification (Fig. 4.9e). Both the surfaces showed mild adhesive and oxidative wear. For example, the presence of microconstituents *$Ni_{0.51}Fe_{0.39}Mo_{0.04}Al_{0.05}Cr_{0.01}O_{0.47}\{B_y\}$* (Figs. 4.9a-b) on the SS surface. Similarly, Ni-30%MoAlB surface showed presence of heterogenous microconstituents, for example, *$Ni_{0.63}Fe_{0.13}M_{o0.11}Al_{0.13}O_{0.78}\{B_y\}$* and *$Ni_{0.77}Fe_{0.10}Mo_{0.05}Al_{0.08}O_{0.45}\{B_y\}$* (Fig. 4.9e).

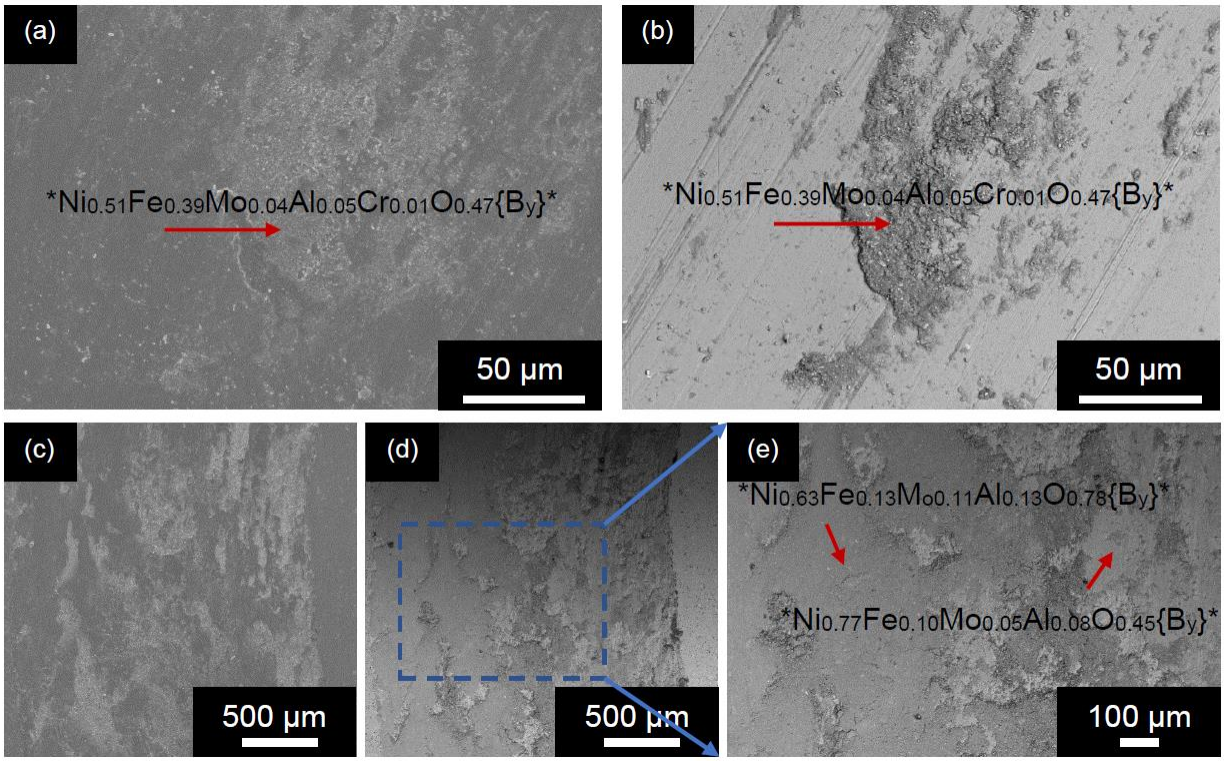


Figure 4.9: SEM micrographs of SS surface in, (a) SE, (b) BSE, and corresponding Ni-30%MoAlB (1550 $^{o}$C) surface in, (c) SE, (d) BSE, and (e) higher magnification of the region highlighted in (d) during dry sliding.

Figures 4.10a-b, and Figs. 4.10c-d show the alumina surface, and the Ni-30%MoAlB (1550 °C) surface after dry sliding, respectively. The tribosurfaces showed signs of abrasive and oxidation wear, and the tribofilms formed on both the surfaces showed microconstituent of similar chemistry of *$Ni_{0.83}Mo_{0.06}Al_{0.10}O_{0.69}\{B_y\}$* (Figs. 4.10a-b) and *$Ni_{0.82}Mo_{0.08}Al_{0.10}O_{0.65}\{B_y\}$* (Figs. 4.10c-d), respectively.

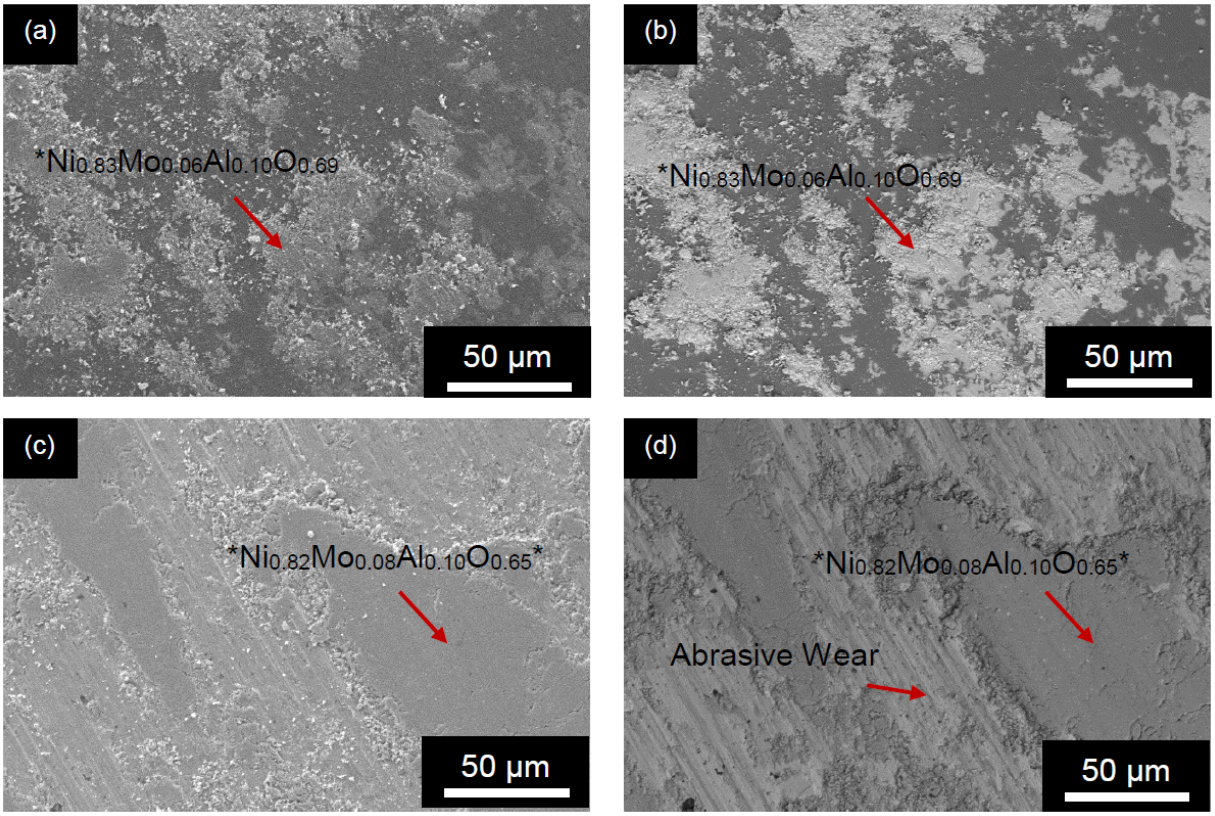


Figure 4.10: SEM micrographs of alumina surface in, (a) SE, (b) BSE, and corresponding Ni-30%MoAlB (1550 °C) surface in, (c) SE, and (d) BSE during dry sliding.

This study clearly shows that the addition of MoAlB particulates are able to decrease the WR of composites by minimizing the adhesive wear between Ni-based metal components, but they are not effective in reducing the abrasive wear against alumina during dry sliding. Most probably, the pull out of MoAlB particulates due to ploughing or abrasive wear during dry sliding leads to higher WR. At this juncture, the exact mechanism is not clear as there has not been a single study on the tribological behavior of MoAlB or its composites.

Table 4.1: Summary of tribological behaviors of different Ni-based coatings and composites.

| Coatings /Compositions | Countersurface | Conditions | WR | μ | Ref. |
|---|---|---|---|---|---|
| Nanocrystalline (nc) Ni with a grain size of 15±3 nm | $Al_2O_3$ ball | Pin-on-disk, 2 N, Ar atmosphere, $3.0\times10^{-2}$ m/s | ~$0.47\times10^{-3}$ | 0.64 | 15 |
| Microcrystalline (mc) Ni with a grain size of 20±5 μm | $Al_2O_3$ ball | Pin-on-disk, 2 N, Ar atmosphere, $3.0\times10^{-2}$ m/s | ~$8.78\times10^{-3}$ | 0.61 | |
| Ni-Co Alloy | $Al_2O_3$ ball | Ball-on-Disk, 1 N, 150 $mms^{-1}$ | ~$0.09 \times 10^{-2}$ | 0.01 | 16 |
| Ni-Co Alloy and 1 g/l MWCT in electrolyte (DC Method) | $Al_2O_3$ ball | Ball-on-Disk, 1 N, 150 $mms_{-1}$ | ~$0.03 \times 10^{-3}$ | 0.1 | |
| Ni with 100 mg/l graphene in electrolyte | M50 Stainless Steel | Ball-on-Disk, 1 N, 100 $mms^{-1}$ | ~$10.17 \times 10^{-4}$ | 0.5 | 17 |
| Ni with 250 mg/l graphene in electrolyte | M50 Stainless Steel | Ball-on-Disk, 1 N, 100 $mms^{-1}$ | ~$9.25 \times 10^{-4}$ | 0.2 | |
| Ni with 500 mg/l graphene in electrolyte | M50 Stainless Steel | Ball-on-Disk, 1 N, 100 $mms^{-1}$ | ~$8.56 \times 10^{-4}$ | 0.15 | |
| PS300 (NiCr-$Cr_2O_3$ (80.3 vol%), Ag (5.5 vol%), $CaF_2/BaF_2$ (14.2 vol%)) | $Al_2O_3$ (pin) | Pin-on-disk, RT, 4.91 N, and 1 m/s | ~$2.3 \times 10^{-4}$ (total wear) | 0.62 | 18 |
| PS400 (NiMoAl (70 wt%)-$Cr_2O_3$ (20 wt%)-Ag (5 wt%) -$BaF_2/CaF_2$(5 wt%)) | Inconel X-750 (pin) | Pin-on-disk, RT, 4.91 N, and 3 m/s after previous sliding at 500 °C and 650 °C | ~$1.2 \times 10^{-3}$ (total wear) | 0.31 | 19 |
| NAF5 (Ni15Cr12Mo3Ti1Al–12.5%Ag–5%$BaF_2/CaF_2$) | $Si_3N_4$ ball | Ball-on-Disk, RT, 5 N, 1 m/s, and 30 min test | ~$6 \times 10^{-5}$ (WR of NAF5) | 0.3 | 20 |

Table 4.1 summarizes the tribological behavior of different types of Ni-based coatings and solid lubricants for example, PS 300, PS 400, and NAF5 coatings against different substrates [15-20]. It is quite difficult to directly compare the tribology data as these tests are done under different conditions which are summarized in Table 4.1. Qualitatively, by inspecting the data summarized in Table 4.1, it can be surmised that the WR in most of the tribocouples lie in the range of $10^{-2}$-$10^{-3}$ $mm^3$/N.m when Ni or its alloy is tested against different ceramics countersurface [15, 16], and WR is further decreased in the range of $10^{-3}$-$10^{-5}$ $mm^3$/N.m after adding additives like MWCT

[16], graphene [17], Ag [18-20], and $CaF_2/BaF_2$ [18-20]. These results are comparable to Ni-MoAlB composites where the WR was in the range of $10^{-4}$ $mm^3$/N.m. Thus, it can be summarized that MoAlB particulates can be potentially used as a high performance multifunctional solid lubricant to minimize wear against metallic components, and engineer mechanical behavior of the composites as these are two component systems. Kota et al. [9] also showed that MoAlB is oxidation resistant during static oxidation testing up to at least 1400 °C due to the formation of dense and adherent alumina scales. Clearly, further research is needed to understand the mechanical and tribological behavior of these solids in high temperature environment.

### 4.4 Conclusions

MoAlB particulates were designed by pressureless sintering and ball milling. XRD studies showed that all the powders were predominatly single phase. Ni-matrix composites were subsequently fabricated for the first time by hot pressing the predominantly single phase MoAlB particulates and Ni powders to fabricate different compositions, for example 5 vol% (Ni-5%MoAlB), 10 vol% (Ni-10%MoAlB), 20 vol% (Ni-20%MoAlB), and 30 vol% (Ni-30%MoAlB) MoAlB in the Ni-matrix. Detailed SEM studies showed that MoAlB particulates are well distributed in the Ni-matrix with minimal interfacial reactions. These particulates had a positive effect on the mechanical and tribological performances. By comparing the data for similar porosity of ~17%, it was observed Ni (165 MPa) had a compressive yield strength of ~467.5 MPa as compared to 498 MPa in Ni-10%MoAlB (1550 °C) (240 MPa) which showed that MoAlB particulates are able to improve the yield strength while decreasing the ductility of the samples.

# CHAPTER V

# CONCLUSIONS AND FUTURE STUDIES

## 5.1 Future Studies

To expand upon the presented work, the etching process of the MoAlB particulates could be optimized to result in fully etched MoAlB particulates, or MBenes. Additionally, nano-sized MoAlB particulates could be fabricated and their effect on the mechanical and tribological properties of MRMB's could be studied. Moreover, MoAlB powders could be sintered to result in a dense MoAlB ceramic part.

The subsequent sections will describe preliminary results in efforts to create a new method of MoAlB powder densification. In this study, MoAlB powders were pressurelessly sintered at various temperatures and with a variety of processing methods in attempts to obtain a dense MoAlB ceramic sample.

## 5.2 Experimental

First, MoAlB powders were fabricated by mixing powders of MoB (Part number 12563 (99% pure), Alfa Aesar, Haverhill, MA) and Al powder (Part number 11067 (99.5% pure), Alfa Aesar, Haverhill, MA) in the molar ratio of 1:1.2 by dry ball milling (8000 M mixer Mill, SPEX SamplePrep, Metuchen, NJ) for 5 minutes. Thereafter, the powders were cold pressed, and annealed at 750 °C for 2h at a ramp rate of 10 °C/min. The annealed samples were then heat treated

at a ramp rate of 10 °C/min to 1000 °C, 1250 °C, and 1550 °C, respectively, for 120 minutes in a tube furnace under flowing Ar. XRD analysis was performed to confirm whether the reacted powders were single phase (Fig. 4.2a). Predominantly single phase MoAlB powder was then ball milled and sieved until -325 mesh by using a sieve shaker. Initially, the phase pure MoAlB particulates were ball mixed with a PVA (Polyvinyl alcohol - part number 363138 (98-99% hydrolyzed, $M_w$ 31,000-50,000), Sigma-Aldrich, St. Louis, MO) binder solution (80 wt% DI (distilled) water/20 wt% PVA) in a methacrylate vial with methacrylate balls for 10 seconds and then cold pressed and sintered at a ramp rate of 10 °C/min until the desired temperature. Further sintering efforts were made by dry ball mixing the required ratio of phase pure MoAlB particulates with Ni powders (Part number 43214 (99.8% metals basis), Alfa Aesar, Haverhill, MA) in a methacrylate vial with methacrylate balls for 5 minutes. Following the dry mixing, the powders were mixed with 10 wt% PVA binder solution for 10 seconds with the same methacrylate vial and methacrylate balls. Thereafter, the powders were cold pressed and sintered at a ramp rate of 10 °C/min until the desired temperature.

In addition to sintering phase pure MoAlB powders, $Ti_3SiC_2$ powders (-325 mesh, Kanthal, Hallstahammar, Sweden) were sintered in a similar fashion as the MoAlB compacts. The required ratio of $Ti_3SiC_2$ powders and Ni powders were dry ball mixed with in a methacrylate vial with methacrylate balls for 5 minutes. Following the dry mixing, the powders were mixed with 10 wt% PVA binder solution for 10 seconds with the same methacrylate vial and methacrylate balls. Thereafter, the powders were cold pressed and sintered at a ramp rate of 10 °C/min until the desired temperature. Additionally, MoAlB-$Ti_3SiC_2$ composites were also fabricated by ball mixing the required ratios of phase pure MoAlB powders, $Ti_3SiC_2$ powders and Ni powders in a methacrylate vial with methacrylate balls for 5 minutes. Following the dry mixing, the powders were mixed

with 10 wt% PVA binder solution for 10 seconds with the same methacrylate vial and methacrylate balls. Thereafter, the powders were cold pressed and sintered at a ramp rate of 10 °C/min until the desired temperature.

Finally, a centrifugation process was performed on the MoAlB powders after synthesis. 1 g of phase pure MoAlB powders was mixed with ~15 mL of DI (distilled) water and centrifuged at ~3,000 rpm for 5 min. The resulting filtrate was drained, and fresh DI (distilled) water was added to the residue. The suspension was centrifuged again for 5 min. This process was repeated for 6 cycles, and the remaining particulates were oven dried at ~100 $^{o}$C for 12 hr. After drying, the MoAlB powders were ball milled in an 8001B hardened steel vial with 8001B hardened steel balls for 5 minutes, and the required ratio of centrifuged MoAlB particulates and Ni powders were dry ball mixed in a methacrylate vial with methacrylate balls for 5 minutes. Thereafter, the powders were mixed with PVA binder solution for 10 seconds with the same methacrylate vial and methacrylate balls. The mixed powders were then cold pressed and sintered at a ramp rate of 10 °C/min until the desired temperature.

During this study, 32 different sintering trials were completed, and a set of three samples were fabricated for each individual trial. In this chapter, the following nomenclature will be used to designate the samples: vol%MoAlB-vol%$Ti_3SiC_2$(wt%Ni)(wt%PVA binder solution)(pressure)(MoAlB powder synthesis temperature)(sintering temperature)(time)(MoAlB synthesis Ar gas pressure)(sintering Ar gas pressure), for example, 50vol%MoAlB-50vol%$Ti_3SiC_2$(2wt%Ni)(10wt%PVA)(350 MPa)(1250 °C)(1550 °C)(120 min)(70 kPa)(140 kPa) means that a 50 vol%MoAlB-50 vol%$Ti_3SiC_2$ composite was fabricated with MoAlB powders synthesized at 1250 °C under ~70 kPa Ar flow, 2 wt% Ni powders as a sintering agent, ~10 wt%

PVA solution used as a binder, cold pressed at ~350 MPa, and sintered at 1550 °C for 120 minutes under ~140 kPa Ar flow. Each respective sintering trial is listed in Table 5.1.

Relative density was determined by dividing the experimental density with theoretical density. The experimental density of the composites was measured from the mass and dimensions of each sample. Rule of mixture was used to calculate the theoretical density of all the composite samples by using the nominal composition, theoretical density of MoAlB, $Ti_3SiC_2$ and Ni particulates. The sintered samples were then machined by a diamond saw into ~3 mm cubes for mechanical testing. All the samples were then tested in compression by using a mechanical testing unit (Shimadzu AD-IS UTM, Shimadzu Scientific Instruments Inc., Columbia, MD) at a deflection rate of 1 mm/min. For each composition, a set of 5 samples were tested.

**5.3 Results and Discussion**

Despite the many modifications to the sintering methods, a dense sintered MoAlB compact was not achieved. Trials #1-3 yielded very low density samples, and thus the cold pressing pressures and sintering temperatures were increased in trials #4-9. Following trials #1-9, it was realized that MoAlB powders cold pressed at ~350 MPa were denser than the MoAlB powders cold pressed at ~88 MPa and subsequent experiments were only performed with the former cold pressing pressure, unless otherwise noted. Previous studies have shown that addition of Ni powders to the matrix promote higher densification of the samples [1], thus Ni powders were then added as a liquid phase sintering agent in each sample with 1 wt% Ni powders added in trials #10-12, and 2 wt% Ni powders added in trials #12-15. After trials #1-15, it became evident that MoAlB powders synthesized at 1250 °C had consistently became the densest, and subsequent experiments were only performed with MoAlB powders synthesized at 1250 °C. Following trials #16-19, it was

determined that the optimum pre-sintering parameters were: a cold pressing pressure of ~350 MPa with 2 wt% Ni powders as a sintering agent and 10 wt% PVA binder solution. Therefore ensuing experiments were only performed with these parameters.

In attempt to further aid in the sintering of MoAlB powders, $Ti_3SiC_2$ powders were added to the sample matrix. In trials #20-22 & #26-28, MoAlB-$Ti_3SiC_2$ ceramic composites were fabricated, and these samples did attain increased densification in comparison to the sintered MoAlB samples. Additionally, for comparison to the MoAlB-$Ti_3SiC_2$ ceramic composites, pure $Ti_3SiC_2$ ceramic samples were also fabricated in trial #24.

During this study, it was observed though SEM imaging, that some alumina impurities were found in the powders of the sintered compacts. In effort to address this, the Ar flow pressure was increased to ~140 kPa for trials #23, #25, #27, #28, & #30. Additionally, in trial #25, the Ar flow pressure was increased to ~140 kPa during both the synthesis of the 1250 °C MoAlB powders and the sintering of the MoAlB compacts.

Following the sintering trials with increased Ar flow pressure, it was evident that the alumina impurities were still present and preventing densification of the sintered samples. To remove the alumina impurities, a centrifugation process was performed on the MoAlB powders after synthesis in trials #29-32. It was confirmed though SEM and EDS study that the alumina impurities were indeed removed by this centrifugation process. Following trials #29 & #30, grain coarsening of the sintered MoAlB samples was observed. It was conjectured that MoAlB powder agglomeration was occurring during centrifugation; therefore, post centrifugation and drying, the MoAlB powders were ball milled in a hardened steel vial with hardened steel balls in trial #31. After these sintering attempts, it was observed through SEM and EDS study, that MoAlB powder

decomposition was occurring, and a final densification attempt was made by using the centrifuged MoAlB powders and sintering the green compacts at of 1400 °C for 240 minutes. It was hypothesized that the lower temperature would not induce decomposition and the longer heating time would promote densification of the MoAlB powders. Nonetheless, unfortunately all attempts to yield a dense single phase MoAlB compact were unsuccessful.

Figures 5.1 & 5.2 and Table 5.1 below show the preliminary results in the variation in average density and porosity of the sintered compacts. The various sintering processes are also described in the Table 5.1. Initial sintering attempts of MoAlB resulted in a very porous solid; therefore, many modifications were made to the pre-sintering processes in efforts to further densify the powders. Despite these adjustments, a sintered compact of greater than 90% dense could not be achieved in this study. The maximum density of 100vol% MoAlB achieved was 4.98 g/cm$^3$ (76.6% dense). The MoAlB-$Ti_3SiC_2$ composites were able to achieve much greater densities, with 5vol%MoAlB-95vol% $Ti_3SiC_2$ resulting in a 95% dense sintered compact. These composites could potentially possess a variety of exciting properties at ambient and high temperatures, as was shown in previous works with pure MAX phases at ambient and high temperatures [1-5].

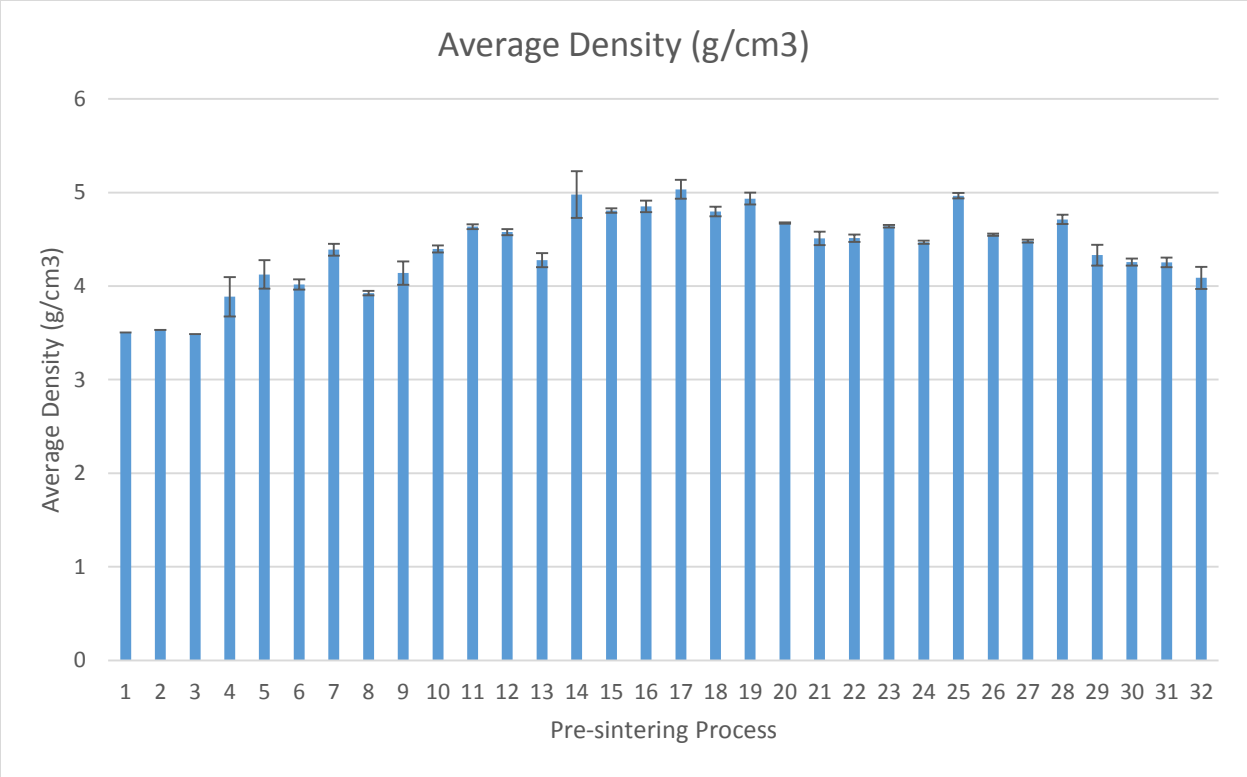


Figure 5.1: Average densities (g/cm$^3$) of various pressureless sintered compacts.

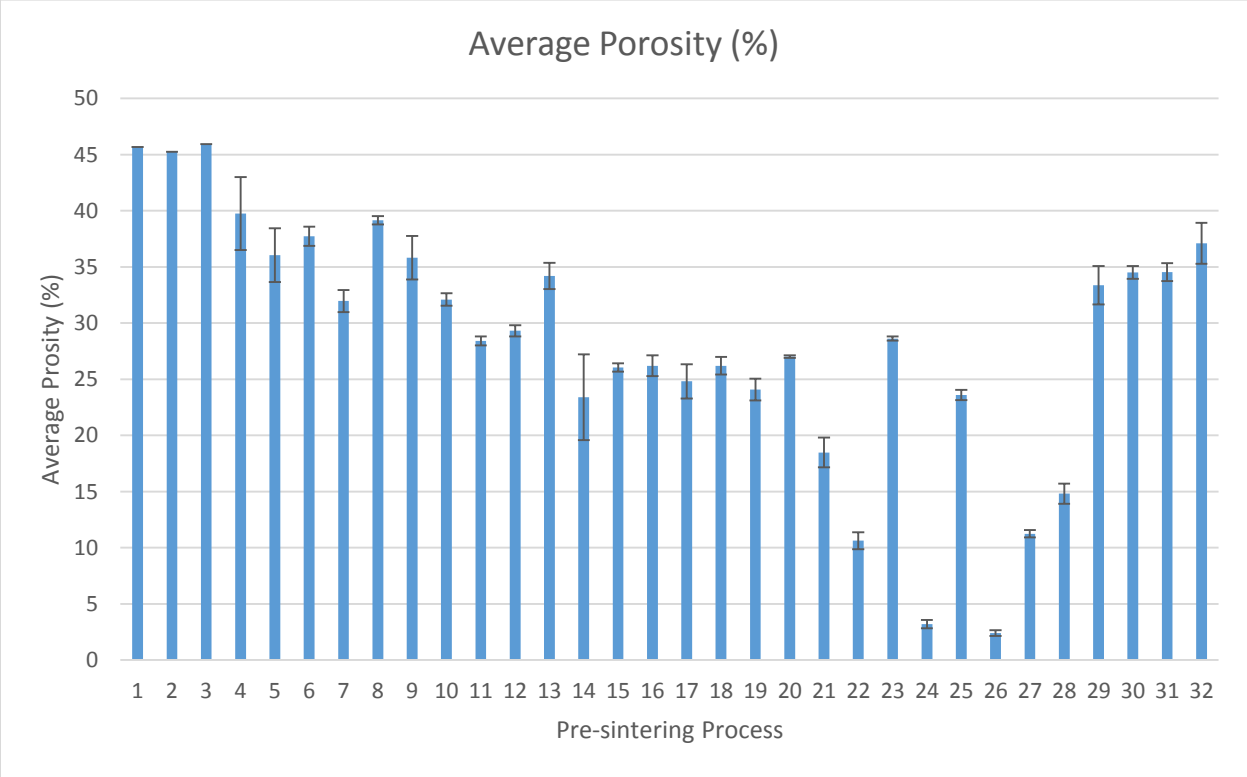


Figure 5.2: Average porosities (%) of various pressureless sintered compacts.

Table 5.1: Description of respective sintering trials, and average densities and porosities of various pressureless sintered compacts.

| Sintering Trial # | Sample Description | Average Density ($g/cm^3$) | Std. ($g/cm^3$) | Average Porosity (%) | Std. (%) |
|---|---|---|---|---|---|
| **1** | 100vol%MoAlB(10wt%PVA)(88 MPa)(1550 °C)(1400 °C)(120 min)(70 kPa)(70 kPa) | 3.51 | - | 45.67 | - |
| **2** | 100vol%MoAlB(10wt%PVA)(88 MPa)(1250 °C)(1400 °C)(120 min)(70 kPa)(70 kPa) | 3.53 | - | 45.27 | - |
| **3** | 100vol%MoAlB(10wt%PVA)(88 MPa)(1000 °C)(1400 °C)(120 min)(70 kPa)(70 kPa) | 3.49 | - | 45.95 | - |
| **4** | 100vol%MoAlB(10wt%PVA)(88 MPa)(1550 °C)(1550 °C)(120 min)(70 kPa)(70 kPa) | 3.89 | 0.21 | 39.76 | 3.24 |
| **5** | 100vol%MoAlB(10wt%PVA)(350 MPa)(1550 °C)(1550 °C)(120 min)(70 kPa)(70 kPa) | 4.12 | 0.15 | 36.05 | 2.38 |
| **6** | 100vol%MoAlB(10wt%PVA)(88 MPa)(1250 °C)(1550 °C)(120 min)(70 kPa)(70 kPa) | 4.02 | 0.06 | 37.74 | 0.86 |
| **7** | 100vol%MoAlB(10wt%PVA)(350 MPa)(1250 °C)(1550 °C)(120 min)(70 kPa)(70 kPa) | 4.39 | 0.06 | 31.96 | 0.99 |
| **8** | 100vol%MoAlB(10wt%PVA)(88 MPa)(1000 °C)(1550 °C)(120 min)(70 kPa)(70 kPa) | 3.92 | 0.02 | 39.15 | 0.37 |
| **9** | 100vol%MoAlB(10wt%PVA)(350 MPa)(1000 °C)(1550 °C)(120 min)(70 kPa)(70 kPa) | 4.14 | 0.12 | 35.82 | 1.94 |
| **10** | 100vol%MoAlB(1wt%Ni)(10wt%PVA)(350 MPa)(1550 °C)(1550 °C)(120 min)(70 kPa)(70 kPa) | 4.40 | 0.04 | 32.09 | 0.56 |
| **11** | 100vol%MoAlB(1wt%Ni)(10wt%PVA)(350 MPa)(1250 °C)(1550 °C)(120 min)(70 kPa)(70 kPa) | 4.64 | 0.03 | 28.41 | 0.39 |
| **12** | 100vol%MoAlB(1wt%Ni)(10wt%PVA)(350 MPa)(1000 °C)(1550 °C)(120 min)(70 kPa)(70 kPa) | 4.58 | 0.03 | 29.31 | 0.49 |
| **13** | 100vol%MoAlB(2wt%Ni)(10wt%PVA)(350 MPa)(1550 °C)(1550 °C)(120 min)(70 kPa)(70 kPa) | 4.28 | 0.08 | 34.21 | 1.17 |
| **14** | 100vol%MoAlB(2wt%Ni)(10wt%PVA)(350 MPa)(1250 °C)(1550 °C)(120 min)(70 kPa)(70 kPa) | 4.98 | 0.25 | 23.40 | 3.83 |

| | | | | | |
|---|---|---|---|---|---|
| **15** | 100vol%MoAlB(2wt%Ni)(10wt%PVA)(350 MPa)(1000 °C)(1550 °C)(120 min)(70 kPa)(70 kPa) | 4.81 | 0.02 | 26.06 | 0.37 |
| **16** | 100vol%MoAlB(5wt%Ni)(10wt%PVA)(350 MPa)(1250 °C)(1550 °C)(120 min)(70 kPa)(70 kPa) | 4.85 | 0.06 | 26.20 | 0.92 |
| **17** | 100vol%MoAlB(10wt%Ni)(10wt%PVA)(350 MPa)(1250 °C)(1550 °C)(120 min)(70 kPa)(70 kPa) | 5.03 | 0.10 | 24.81 | 1.52 |
| **18** | 100vol%MoAlB(2wt%Ni)(10wt%PVA)(700 MPa)(1250 °C)(1550 °C)(120 min)(70 kPa)(70 kPa) | 4.80 | 0.05 | 26.20 | 0.78 |
| **19** | 100vol%MoAlB(2wt%Ni)(5wt%PVA)(700 MPa)(1250 °C)(1550 °C)(120 min)(70 kPa)(70 kPa) | 4.93 | 0.06 | 24.08 | 0.97 |
| **20** | 97vol%MoAlB-3vol%$Ti_3SiC_2$(2wt%Ni)(10wt%PVA)(350 MPa)(1250 °C)(1550 °C)(120 min)(70 kPa)(70 kPa) | 4.67 | 0.01 | 27.02 | 0.11 |
| **21** | 50vol%MoAlB-50vol%$Ti_3SiC_2$(2wt%Ni)(10wt%PVA)(350 MPa)(1250 °C)(1550 °C)(120 min)(70 kPa)(70 kPa) | 4.51 | 0.07 | 18.48 | 1.32 |
| **22** | 25vol%MoAlB-75vol%$Ti_3SiC_2$(2wt%Ni)(10wt%PVA)(350 MPa)(1250 °C)(1550 °C)(120 min)(70 kPa)(70 kPa) | 4.51 | 0.04 | 10.63 | 0.76 |
| **23** | 100vol%MoAlB(2wt%Ni)(10wt%PVA)(350 MPa)(1250 °C)(1550 °C)(120 min)(70 kPa)(140 kPa) | 4.64 | 0.01 | 28.63 | 0.20 |
| **24** | 100vol%$Ti_3SiC_2$(2wt%Ni)(10wt%PVA)(350 MPa)(1250 °C)(1550 °C)(120 min)(70 kPa) | 4.47 | 0.02 | 3.20 | 0.37 |
| **25** | 100vol%MoAlB(2wt%Ni)(10wt%PVA)(350 MPa)(1250 °C)(1550 °C)(120 min)(140 kPa)(140 kPa) | 4.97 | 0.03 | 23.60 | 0.45 |
| **26** | 5vol%MoAlB-95vol%$Ti_3SiC_2$(2wt%Ni)(10wt%PVA)(350 MPa)(1250 °C)(1550 °C)(120 min)(70 kPa)(70 kPa) | 4.55 | 0.01 | 2.40 | 0.25 |
| **27** | 25vol%MoAlB-75vol%$Ti_3SiC_2$(2wt%Ni)(10wt%PVA)(350 MPa)(1250 °C)(1550 °C)(120 min)(70 kPa)(140 kPa) | 4.48 | 0.02 | 11.24 | 0.33 |
| **28** | 50vol%MoAlB-50vol%$Ti_3SiC_2$(2wt%Ni)(10wt%PVA)(350 MPa)(1250 °C)(1550 °C)(120 min)(70 kPa)(140 kPa) | 4.71 | 0.05 | 14.81 | 0.90 |

| | | | | | |
|---|---|---|---|---|---|
| **29** | 100vol% centrifuged MoAlB(2wt%Ni)(10wt%PVA)(350 MPa)(1250 °C)(1550 °C)(120 min)(70 kPa)(70 kPa) | 4.33 | 0.11 | 33.38 | 1.71 |
| **30** | 100vol% centrifuged MoAlB(2wt%Ni)(10wt%PVA)(350 MPa)(1250 °C)(1550 °C)(120 min)(70 kPa)(140 kPa) | 4.26 | 0.04 | 34.51 | 0.57 |
| **31** | 100vol% centrifuged, ball milled MoAlB(2wt%Ni)(10wt%PVA)(350 MPa)(1250 °C)(1550 °C)(120 min)(70 kPa)(70 kPa) | 4.25 | 0.05 | 34.54 | 0.79 |
| **32** | 100vol% centrifuged MoAlB(2wt%Ni)(10wt%PVA)(350 MPa)(1250 °C)(1400 °C)(240 min)(70 kPa)(70 kPa) | 4.09 | 0.12 | 37.10 | 1.81 |

After the compacts were sintered, they were polished and cut into cubes with cross sectional dimensions of ~3mm x ~3mm. Figure 5.3 and Table 5.2 below show the variation in average compressive yield strengths of the sintered compacts. Sintering trials #1-9 and #29-32 were not compression tested due to their very low relative densities. These preliminary results show that, in general, the yield strengths of the sintered compacts increased as their density increased; however, due to the presence of large pores in the samples, there is a large variance in the results. More studies are needed to be conducted to improve the densities of these sintered compacts and obtain a better understanding of their properties.

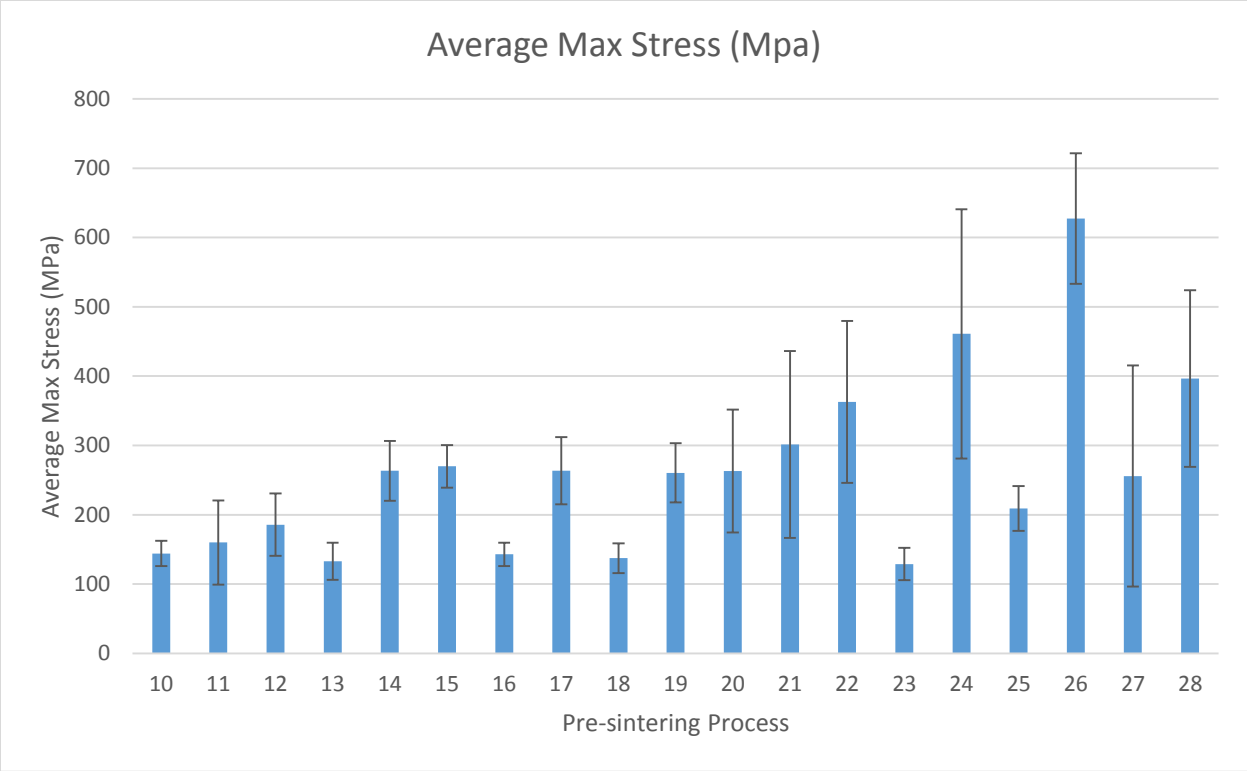


Figure 5.3: Average maximum stresses (MPa) of various pressureless sintered compacts.

Table 5.2: Average compressive strengths of various pressureless sintered compacts.

| Sintering Trial # | Sample Description | Average Compressive Stress (MPa) | Std. (MPa) |
|---|---|---|---|
| **10** | 100vol%MoAlB(1wt%Ni)(10wt%PVA)(350 MPa)(1550 °C)(1550 °C)(120 min)(70 kPa)(70 kPa) | 143.99 | 18.29 |
| **11** | 100vol%MoAlB(1wt%Ni)(10wt%PVA)(350 MPa)(1250 °C)(1550 °C)(120 min)(70 kPa)(70 kPa) | 159.90 | 60.87 |
| **12** | 100vol%MoAlB(1wt%Ni)(10wt%PVA)(350 MPa)(1000 °C)(1550 °C)(120 min)(70 kPa)(70 kPa) | 185.59 | 45.11 |
| **13** | 100vol%MoAlB(2wt%Ni)(10wt%PVA)(350 MPa)(1550 °C)(1550 °C)(120 min)(70 kPa)(70 kPa) | 133.00 | 26.77 |
| **14** | 100vol%MoAlB(2wt%Ni)(10wt%PVA)(350 MPa)(1250 °C)(1550 °C)(120 min)(70 kPa)(70 kPa) | 263.29 | 43.17 |
| **15** | 100vol%MoAlB(2wt%Ni)(10wt%PVA)(350 MPa)(1000 °C)(1550 °C)(120 min)(70 kPa)(70 kPa) | 269.76 | 30.63 |
| **16** | 100vol%MoAlB(5wt%Ni)(10wt%PVA)(350 MPa)(1250 °C)(1550 °C)(120 min)(70 kPa)(70 kPa) | 142.75 | 16.71 |
| **17** | 100vol%MoAlB(10wt%Ni)(10wt%PVA)(350 MPa)(1250 °C)(1550 °C)(120 min)(70 kPa)(70 kPa) | 263.50 | 48.31 |

| | | | |
|---|---|---|---|
| **18** | 100vol%MoAlB(2wt%Ni)(10wt%PVA)(700 MPa)(1250 °C)(1550 °C)(120 min)(70 kPa)(70 kPa) | 137.35 | 21.53 |
| **19** | 100vol%MoAlB(2wt%Ni)(5wt%PVA)(700 MPa)(1250 °C)(1550 °C)(120 min)(70 kPa)(70 kPa) | 260.42 | 42.70 |
| **20** | 97vol%MoAlB-3vol%$Ti_3SiC_2$(2wt%Ni)(10wt%PVA)(350 MPa)(1250 °C)(1550 °C)(120 min)(70 kPa)(70 kPa) | 262.96 | 88.57 |
| **21** | 50vol%MoAlB-50vol%$Ti_3SiC_2$(2wt%Ni)(10wt%PVA)(350 MPa)(1250 °C)(1550 °C)(120 min)(70 kPa)(70 kPa) | 301.29 | 134.79 |
| **22** | 25vol%MoAlB-75vol%$Ti_3SiC_2$(2wt%Ni)(10wt%PVA)(350 MPa)(1250 °C)(1550 °C)(120 min)(70 kPa)(70 kPa) | 362.64 | 116.92 |
| **23** | 100vol%MoAlB(2wt%Ni)(10wt%PVA)(350 MPa)(1250 °C)(1550 °C)(120 min)(70 kPa)(140 kPa) | 128.86 | 23.12 |
| **24** | 100vol%$Ti_3SiC_2$(2wt%Ni)(10wt%PVA)(350 MPa)(1250 °C)(1550 °C)(120 min)(70 kPa) | 460.97 | 179.97 |
| **25** | 100vol%MoAlB(2wt%Ni)(10wt%PVA)(350 MPa)(1250 °C)(1550 °C)(120 min)(140 kPa)(140 kPa) | 209.01 | 32.53 |
| **26** | 5vol%MoAlB-95vol%$Ti_3SiC_2$(2wt%Ni)(10wt%PVA)(350 MPa)(1250 °C)(1550 °C)(120 min)(70 kPa)(70 kPa) | 627.35 | 94.07 |
| **27** | 25vol%MoAlB-75vol%$Ti_3SiC_2$(2wt%Ni)(10wt%PVA)(350 MPa)(1250 °C)(1550 °C)(120 min)(70 kPa)(140 kPa) | 255.84 | 159.34 |
| **28** | 50vol%MoAlB-50vol%$Ti_3SiC_2$(2wt%Ni)(10wt%PVA)(350 MPa)(1250 °C)(1550 °C)(120 min)(70 kPa)(140 kPa) | 396.42 | 127.49 |

### 5.4 Conclusions

Various MAX phase particulates ($Cr_2AlC$, $Cr_2GaC$, and $V_2AlC$) were synthesized via pressureless reaction; in addition, the particle size of $Ti_3SiC_2$ particles were engineered by ball milling. Furthermore, novel MoAlB powders were synthesized via pressureless reaction at various reaction temperatures, and MABene particulates were fabricated from these MoAlB particulates. These powders were then characterized using XRD, SEM, and EDS analyses. Finally, novel Ni-MoAlB (MRMB) composites were manufactured and their mechanical and tribological properties were analyzed.

The studies show that various MAX phase powders can be successfully synthesized via pressureless reaction, and that their particle sizes can be engineered by ball milling. Additionally,

it was shown that MAB phase powders, in particular MoAlB, can be successfully synthesized via pressureless reaction at various temperatures (1000 °C – 1550 °C). The synthesis of etched MAB phase particulates (MABenes) and Ni-MoAlB (MRMB) composites were then reported for the first time in literature. The mixing of MAB phases with HCl and LiF solution caused the aluminum layer of MoAlB to be partially etched from the MoAlB powders, resulting in MABene particulates which could potentially hold exciting properties similar to that of MXenes. Synthesis and analysis of the Ni-MoAlB (MRMB) composites showed improved tribological performances against stainless steel, and relatively constant yield strengths despite the increases in porosities as more MoAlB powders were added to the Ni matrix. Finally, preliminary results show that MoAlB-$Ti_3SiC_2$ composites can be successfully fabricated via pressureless sintering.

Although these results are not fully optimized, they show great promise for MoAlB to be used as a multifunctional material and as a solid lubricant additive in metal-MRMB tribocouples. An exciting potential use for such a material would be in vehicle engines, such as if a military helicopter gets shot over a desert and loses its engine oil, the engine could still run for a period of time allowing for the helicopter to return to safety. Furthermore, etched MoAlB could possess various other thrilling properties not exhibited by MoAlB, such as energy storage capabilities or enhanced mechanical and tribological behaviors. The results presented in this work warrant further study of MAB phases and MABenes for their effect on mechanical and tribological properties of MRMB composites.

# APPENDIX

## Status of Journal Publications

1. "Design and Synthesis of Novel Nano-laminated Particulates for Fabricating Novel Multifunctional Composites", M. Fuka, F. AlAnazi, S. Ghosh, and S. Gupta, IJIRSET, 2016, DOI:10.15680/IJIRSET.2016.0512138.

2. "Synthesis of MoAlB Particulates and Their Porous Derivatives by Selective Deintercalation of Al from MoAlB", S. Gupta, M. Fuka, In: Sun Z. et al. (eds) Energy Technology 2018. TMS 2018. The Minerals, Metals & Materials Series. Springer, Cham (2018).

3. "Novel Ternary Boride (MoAlB) Particulates as Solid Lubricant Additives in Ni-Matrix Composites", M. Fuka, M. Dey, S. Gupta, 2018 Joint Propulsion Conference, AIAA Propulsion and Energy Forum and Exposition (accepted).

4. "Synthesis and Characterization of Novel Ni-$Ti_3SiC_2$ Composites", M. Dey, M. Fuka, F. AlAnazi, and S. Gupta, Proceedings of 42nd Int'l Conf & Expo on Advanced Ceramics & Composites (ICACC 2018) (submitted).

## Contributed Presentations during Master's Degree

1. "On the Development of Novel Multifunctional MAX Reinforced Polymers (MRPs) Matrix Composites", M. Fuka, S. Ghosh, F. AlAnazi, M. Dey, S. Gupta, Graduate Student Seminar, UND, 2017.

2. "On the Development of Novel Multifunctional MAX Reinforced Polymers (MRPs) Matrix Composites", S. Ghosh, M. Fuka, F. AlAnazi, S. Gupta, ICACC 2017, Daytona Beach, Florida.

3. "On the Design of Novel MAX-Polymer (MAXPOL) Multifunctional Composites", M. Fuka, F. AlAnazi, M. Dey, K. Hall, S. Gupta, UND GRADay, 2017.

4. "Creating Materials for Oil Free Engines", M. Fuka, S. Gupta, Three Minute Thesis, UND, 2017.

5. "Novel MAX-Polymer (MAXPOL) Multifunctional Composites", M. Fuka, S. Ghosh, F. AlAnzai, R. Dunnigan, S. Gupta, 2017 ND EPSCoR, Fargo, North Dakota.

6. “Synthesis of MoAlB/MABene Particulates and Their Use as Multifunctional Additives in Ni-Matrix Composites”, M. Fuka, M. Dey, S. Gupta, Graduate Student Seminar, UND, 2017.

7. “Synthesis and Characterization of Novel Ni-MAB Composites”, M. Fuka, M. Dey, S. Gupta, ICACC 2018, Daytona Beach, Florida.

8. "A Review of Different Types of MAX-Metal Composite Systems for Multifunctional Applications”, M. Dey, M. Fuka, S. Gupta, ICACC 2018, Daytona Beach, Florida.

9. “Design of Novel Ni-$Ti_3SiC_2$ Based Multilayer Composites”, Q. Tran, M. Fuka, M. Dey, S. Gupta, ICACC 2018, Daytona Beach, Florida.

10. “Synthesis and Characterization of Novel Ni-MoAlB Composites”, M. Fuka, M. Dey, S. Gupta, UND GRADay, 2018.

11. “Novel Ternary Boride (MoAlB) Particulates as Solid Lubricant Additives in Ni-Matrix Composites”, M. Fuka, M. Dey, S. Gupta, 2018 ND EPSCoR, Grand Forks, North Dakota.

# REFERENCES

## CHAPTER I


[1] W. Shizhu and H. Ping, "Principles of Tribology", John Wiley & Sons, 7-11, 439-450, (2012).

[2] W. Gross, L. Matsch, V. Castelli, A. Eshel, J. Vohr and M. Wildmann, "Fluid Film Lubrication", John Wiley & Sons, 66, 718, (1980).

[3] Q. Luo, "Tribofilms in Solid Lubricants", In: Wang Q.J., Chung YW. (eds) Encyclopedia of Tribology. Springer, (2013).

[4] F. Clauss, "Solid Lubricants and Self-Lubricating Solids", 1st ed. Academic Press, Inc., 15-112 (1972).

[5] H. Harani, "Fundamentals of Engineering Tribology with Applications", 1st ed. Cambridge University Press, 22 (2016).

[6] M.W. Barsoum, "MAX Phases: Properties of Machinable Ternary Carbides and Nitrides", 1st ed. Wiley-VCH, 1-10, 403-410 (2013).

[7] M.W. Barsoum and T. El-Raghy, "The MAX Phases: Unique New Carbide and Nitride Materials", American Scientist, 89, 334-343 (2001).

[8] M.W. Barsoum and T. El-Raghy, "Synthesis and Characterization of a Remarkable Ceramic: $Ti_3SiC_2$", Journal of the American Ceramic Society, 79, 1953-1956 (1996).

[9] S. Gupta and M.W. Barsoum, "On the tribology of the MAX phases and their composites during dry sliding: A review", Wear, 271, 1878-1894 (2011).

[10] S. Gupta, D. Filimonov, V. Zaitsev, T. Palanisamy, and M.W. Barsoum, "Ambient and 550 °C tribological behavior of select MAX phases against Ni-based superalloys", Wear, (2007).

[11] S. Gupta, D. Filimonov, T. Palanisamy, and M.W. Barsoum, "Tribological behavior of select MAX phases against $Al_2O_3$ at elevated temperatures", Wear, 265, 560-565 (2008).

[12] M. Naguib, M. Kurtoglu, V. Presser, J. Lu, J. Niu, M. Heon, L. Hultman, Y. Gogotsi, and M.W. Barsoum, "Two-Dimensional Nanocrystals Produced by Exfoliation of $Ti_3AlC_2$", Advanced Materials, 23, 4248-4253 (2011).

[13] M. Naguib, V.N. Mochalin, M.W. Barsoum, and Y. Gogotsi, "25th Anniversary Article: MXenes: A New Family of Two-Dimensional Materials", Advanced Materials, 26, 992-1005 (2014).

[14] B. Anasori, M.R. Lukatskaya, and Y. Gogotsi, "2D metal carbides and nitrides (MXenes) for energy storage", Nature Reviews, 2:16098 (2017).

[15] S. Okada, K. Iizumi, K. Kudaka, K. Kudou, M. Miyamoto, Y. Yu, and T. Lundström, "Single Crystal Growth of $(Mo_XCr_{1-X})AlB$ and $(Mo_XW_{1-X})AlB$ by Metal Al Solutions and Properties of the Crystals", Journal of Solid State Chemistry, 133, 36-43 (1997).

[16] M. Ade and H. Hillebrecht, "Ternary Borides $Cr_2AlB_2$, $Cr_3AlB_4$, and $Cr_4AlB_6$: The First Members of the Series $(CrB_2)_nCrAl$ with n = 1, 2, 3 and a Unifying Concept for Ternary Borides as MAB-Phases" Inorganic Chemisty, 54, 6122-6135 (2015).

[17] S. Kota, E. Zapata-Solvas, A. Ly, J. Lu, O. Elkassabany, A. Huon, W.E. Lee, L. Hultman, S.J. May, and M.W. Barsoum, "Synthesis and Characterization of an Alumina Forming Nanolaminated Boride: MoAlB", Scientific Reports, 6:26475 (2016).

[18] S. Gupta, D. Filimonov, T. Palanisamy, T. El-Raghy, M.W. Barsoum, "$Ta_2AlC$ and $Cr_2AlC$ Ag-based composites—New solid lubricant materials for use over a wide temperature range against Ni-based superalloys and alumina", Wear, 262, 1479–1489 (2007).

[19] S. Gupta, T. Hammann, R. Johnson, and M.F. Riyad, "Synthesis and Characterization of Novel Al-Matrix Composites Reinforced with $Ti_3SiC_2$ Particulates", Journal of Materials Engineering and Performance, 24, 1011-1017 (2014).

[20] T. Hammann, R. Johnson, M. F. Riyad, and S. Gupta, "Novel Ti3SiC2 reinforced Sn matrix composites", Proceedings of 39th International Conference & Expo on Advanced Ceramics & Composites (ICACC 2015).

[21] S. Gupta, M.A. Habib, R. Dunnigan, et al., "Synthesis and Characterization of Ti3SiC2 Particulate-Reinforced Novel Zn Matrix Composites", J. of Materi Eng and Perform, 24, 4071-4076 (2015).

[22] S. Gupta, F. AlAnazi, S. Ghosh, R. Dunnigan, "Synthesis and Tribological Behavior of Novel Ag- and Bi- Based Composites Reinforced with $Ti_3SiC_2$", Wear, 376, 1074-1083 (2017).

[23] ", Q. Tran, M. Fuka, M. Dey, and S. Gupta, "Design of Novel Ni-$Ti_3SiC_2$ based Multilayered Composites Proceedings of 42nd International Conference & Expo on Advanced Ceramics & Composites (ICACC 2018).

[24] S. Gupta, T. Hammann, R. Johnson, M.F. Riyad, "Tribological Behavior of Novel Ti3SiC2 (Natural Nanolaminates)-Reinforced Epoxy Composites during Dry Sliding", Tribology Transactions, 58, 560–566 (2015).

[25] S. Gupta, S. Ghosh, and R. Dunnigan, "Synthesis and Tribological Behavior of Novel Wear Resistant PEEK-Ti3SiC2 composites", Journal of Engineering Tribology, 231, 422-428 (2017).

[26] S. Ghosh, R. Dunnigan, M.A. Habib, and S. Gupta, "Novel MAX-Polymer Multifunctional Composites", Proceedings of 40th International Conference & Expo on Advanced Ceramics & Composites (ICACC 2016).

## CHAPTER II


[1] M.W. Barsoum, "MAX Phases: Properties of Machinable Ternary Carbides and Nitrides", John Wiley & Sons (2013).

[2] M.W. Barsoum and M. Radovic, "Elastic and Mechanical Properties of the MAX Phases", Annu. Rev. Mater. Res. **41**, 195-227 (2011).

[3] M.W. Barsoum, T. El-Raghy, "Synthesis and characterization of a remarkable ceramic: $Ti_3SiC_2$", J. Am. Ceram. Soc. **79**, 1953–1956 (1996).

[4] M.W. Barsoum, "The $M_{n+1}AX_n$ phases: a new class of solids; thermodynamically stable nanolaminates", Prog. Solid State Chem. **28**, 201–281 (2000).

[5] S. Amini, M.W. Barsoum, T. El-Raghy, "Synthesis and mechanical properties of fully dense $Ti_2SC$", J. Am. Ceram. Soc. **90** (12), 3953–3958 (2007).

[6] B. Anasori, S. Amini, V. Presser, and M.W. Barsoum, "Nanocrystalline Mg-matrix composites with ultrahigh damping properties", Magnesium Technology, John Wiley and Sons, Inc, 463-468 (2011).

[7] W.J. Wang, V. Gauthier-Brunet, G.P. Bei, G. Laplanche, J. Bonneville, A. Joulain, S. Dubois, "Powder metallurgy processing and compressive properties of $Ti_3AlC_2$/Al composites", Mater. Sci. Eng. A **530**, 168–173 (2011).

[8] L. Hu, A. Kothalkar, M. O'Neil, I. Karaman, M. Radovic, "Current-activated, pressure-assisted infiltration: a novel, versatile route for producing interpenetrating ceramic–metal composites", Mater. Res. Lett. (2014), http://dx.doi.org/10.1080/21663831.2013.873498

[9] A. Kothalkar, R. Benitez, L. Hu, M. Radovic, I. Karaman, "Thermo-mechanical response and damping behavior of shape memory alloy/MAX phase composites", Metall. Mater. Trans. A. 45, 2646–2658 (2014).

[10] M.T. Agne, M. Radovic, G.W. Bentzel, M.W. Barsoum, "Stability of $V_2AlC$ with Al in 800-1000C temperature range and ***in situ*** synthesis of $V_2AlC$/Al composites"**,** J. Alloys Compd., **666**, 279-286 (2016).

[11] S. Gupta, T. Hammann, R. Johnson, and M.F. Riyad, "Synthesis and Characterization of Novel Al-Matrix Composites Reinforced with $Ti_3SiC_2$ Particulates", Journal of Materials Engineering and Performance, 24, 1011-1017 (2014).

[12] T. Hammann, R. Johnson, M.F. Riyad, and S. Gupta, "Effect of $Ti_3SiC_2$ Particulates on The Mechanical and Theological Behavior of Sn Matrix Composites", Proceedings of 39th Int'l Conf & Expo on Advanced Ceramics & Composites (ICACC 2015).

[13] S. Gupta, Habib, M.A., R. Dunnigan, et al., "Synthesis and Characterization of $Ti_3SiC_2$ Particulate-Reinforced Novel Zn Matrix Composites", J. Mater. Eng. Perform., **24**, 4071-4076 (2015).

[14] M. Xue, X. Zhang, H. Tang and C. Li, "Synthesis of high purity $Cr_2AlC$ nanolamellas with improved tribological properties for oil-based additives", ***RSC Adv.***, **4**, 39280-39286 (2014).

[15] Z. Su, S. Zeng, J. Zhou et al., "Synthesis and characterization of $Cr_2AlC$ with nanolaminated particles", Chin. Sci. Bull., **59**, 3266-3270 (2014) doi:10.1007/s11434-014-0315-5.

[16] D.T. Cuskelly, E.H. Kisi, "Single-Step Carbothermal Synthesis of High-Purity MAX Phase Powders", J. Am. Ceram. Soc., **99**, 1137-1140 (2016)

[17] M. Naguib, R. R. Unocic, B. L. Armstrong and J. Nanda, "Large-scale delamination of multi-layers transition metal carbides and carbonitrides "MXenes"", Dalton Trans.**, 44**, 9353-9358 (2015).

**CHAPTER III**

[1] F. Koppens, et al., "Photodetectors based on graphene, other two-dimensional materials and hybrid systems", Nat. Nanotechnol., **9**, 780–793 (2014).

[2] Bhimanapati et al., "Recent Advances in Two-Dimensional Materials beyond Graphene", ACS Nano, 9, 11509–11539 (2015).

[3] V. Nicolosi, M. Chhowalla, M. G Kanatzidis, M. S. Strano, and J. N. Coleman, "Liquid exfoliation of layered materials", *Science* **340**, 1226419 (2013).

[4] B. Lalmi, H. Oughaddou, H. Enriquez, A. Kara, S. Vizzini, B. Ealet, and B. Aufray, "Epitaxial growth of a silicene sheet", APPLIED PHYSICS LETTERS **97**, 223109 (2010).

[5] M E Dávila, L Xian, S Cahangirov, A Rubio, and G Le Lay, "Germanene: a novel two-dimensional germanium allotrope akin to graphene and silicone", New Journal of Physics 16 (2014) 095002.

[6] H. Liu, A. T. Neal, Z. Zhu, Z. Luo, X. Xu, D. Tomanek, and P. D. Ye, "Phosphorene: An Unexplored 2D Semiconductor with a High Hole Mobility", ACS Nano, 8, 4033–4041 (2014).

[7] C. Tan and H. Zhang, "Two-dimensional transition metal dichalcogenide nanosheet-based composites", Chem. Soc. Rev., 2015, 44, 2713.

[8] C. Ataca, H.Sahin, and S. Ciraci, "Stable, single-layer $MX_2$ transition-metal oxides and dichalcogenides in a honeycomb-like structure", *J. Phys. Chem. C* **116**, 8983–8999 (2012).

[9] B. Anasori, M. R. Lukatskaya and Y. Gogotsi, "2D metal carbides and nitrides (MXenes) for energy storage", *Nature Reviews*, VOLUME 2 | ARTICLE NUMBER 16098.

[10] M. Naguib, et al., "Two-dimensional nanocrystals produced by exfoliation of $Ti_3AlC_2$", *Adv. Mater.* **23**, 4248–4253 (2011).

[11] M.W. Barsoum, "MAX Phases: Properties of Machinable Ternary Carbides and Nitrides", John Wiley & Sons (2013).

[12] M.W. Barsoum and M. Radovic, "Elastic and Mechanical Properties of the MAX Phases", Annu. Rev. Mater. Res. **41**, 195-227 (2011).

[13] M.W. Barsoum, T. El- Raghy, "Synthesis and characterization of a remarkable ceramic: $Ti_3SiC_2$", J. Am. Ceram. Soc. **79**, 1953–1956 (1996).

[14] M.W. Barsoum, "The $M_{n+1}AX_n$ phases: a new class of solids; thermodynamically stable nanolaminates", Prog. Solid State Chem. **28**, 201–281 (2000).

[15] M. R. Lukatskaya, M. Q. Zhao, Y. Gogotsi, & M. W. Barsoum, "Conductive two dimensional titanium carbide 'clay' with high volumetric capacitance", Ghidiu, *Nature* **516**, 78–81 (2014).

[16] R. Meshkian et al., "Synthesis of two-dimensional molybdenum carbide, $Mo_2C$, from the gallium based atomic laminate $Mo_2Ga_2C$", *Scripta Mater.* **108**, 147–150 (2015).

[17] W. Jeitschko, "Die Kristallstruktur von MoAlB", *Monatshefte für Chemie und verwandte Teile anderer Wissenschaften* **97,** 1472–147 (1966).

[18] W. Jeitschko, "The crystal structure of $Fe_2AlB_2$", *Acta Crystallogr. Sect. B Struct. Crystallogr. Cryst. Chem.* **25,** 163–165 (1969).

[19] M. Ade and H. Hillebrecht, "Ternary Borides $Cr_2AlB_2$, $Cr_3AlB_4$ , and $Cr_4AlB_6$: The First Members of the Series $(CrB_2)_nCrAl$ with n = 1,2, 3 and a Unifying Concept for Ternary Borides as MAB-Phases", *Inorg. Chem.* **54,** 6122–6135 (2015).

[20] S. Kota, E. Zapata-Solvas, A. Ly, J. Lu, O. Elkassabany, A. Huon, W. E. Lee, L. Hultman, S.J. May & M. W. Barsoum, "Synthesis and Characterization of an Alumina Forming Nanolaminated Boride: MoAlB", Scientific Reports**,** 6:26475, DOI: 10.1038/srep26475.

[21] C. A Schneider, W. S Rasband, & K. W. Eliceiri, "NIH Image to ImageJ: 25 years of image analysis", Nature Methods, **9**, 671–675 (2012).

**CHAPTER IV**

[1] M.W. Barsoum and M. Radovic, "Elastic and Mechanical Properties of the MAX Phases", Annu. Rev. Mater. Res. **41**, 195-227 (2011).

[2] M.W. Barsoum, T. El- Raghy, "Synthesis and characterization of a remarkable ceramic: $Ti_3SiC_2$", J. Am. Ceram. Soc. **79**, 1953–1956 (1996).

[3] M.W. Barsoum, "The $M_{n+1}AX_n$ phases: a new class of solids; thermodynamically stable nanolaminates", Prog. Solid State Chem. **28**, 201–281 (2000).

[4] S. Amini, M.W. Barsoum, T. El- Raghy, "Synthesis and mechanical properties of fully dense $Ti_2SC$", J. Am. Ceram. Soc. **90** (12), 3953–3958 (2007).

[5] W. Jeitschko, "Die Kristallstruktur von MoAlB", *Monatshefte für Chemie und verwandte Teile anderer Wissenschaften* **97,** 1472–147 (1966).

[6] W. Jeitschko, "The crystal structure of $Fe_2AlB_2$", *Acta Crystallogr. Sect. B Struct. Crystallogr Cryst. Chem.* **25,** 163–165 (1969).

[7] S. Okada, K. Iizumi, K. Kudaka, K. Kudou, M. Miyamoto, Y. Yu, and T. Lundstrom, "Single Crystal Growth of $(Mo_xCr_{1-x})AlB$ and $(Mo_xW1_{-x})AlB$ by Metal Al Solutions and Properties of the Crystals", J. Solid State Chem. **133**, 36–43 (1997).

[8] M. Ade and H. Hillebrecht, "Ternary Borides $Cr_2AlB_2$, $Cr_3AlB_4$, and $Cr_4AlB_6$: The First Members of the Series $(CrB_2)_nCrAl$ with n = 1,2, 3 and a Unifying Concept for Ternary Borides as MAB-Phases", *Inorg. Chem.* **54,** 6122–6135 (2015).

[9] S. Kota, E. Zapata-Solvas, A. Ly, J. Lu, O. Elkassabany, A. Huon, W. E. Lee, L. Hultman, S. J. May & M. W. Barsoum, "Synthesis and Characterization of an Alumina Forming Nanolaminated Boride: MoAlB", Scientific Reports**,** 6:26475, DOI: 10.1038/srep26475.

[10] S. Gupta, T. Hammann, R. Johnson, and M.F. Riyad, "Synthesis and Characterization of Novel Al-Matrix Composites Reinforced with $Ti_3SiC_2$ Particulates", Journal of Materials Engineering and Performance, 24, 1011-1017 (2014).

[11] S. Gupta, Habib, M.A., R. Dunnigan et al., "Synthesis and Characterization of $Ti_3SiC_2$ Particulate-Reinforced Novel Zn-Matrix Composites", J. of Materi Eng and Perform (2015) 24: 4071.

[12] F. AlAnazi, S. Ghosh, R. Dunnigan, and S. Gupta, "Synthesis and Tribological Behavior of Novel Ag- and Bi-based Composites Reinforced with $Ti_3SiC_2$*"*, Wear **376-377** (2017) 1074–1083.

[13] M. Dey, M. Fuka, F. AlAnazi, and S. Gupta, "Synthesis and Characterization of Novel Ni-$Ti_3SiC_2$ Composites", Proceedings of 42nd Int'l Conf & Expo on Advanced Ceramics & Composites (ICACC 2018) (submitted).

[14] H. Lia, L.M. Peng, M. Gong, L.H. Heb, J.H. Zhaob , and Y.F. Zhang, "Processing and microstructure of $Ti_3SiC_2$/M (M = Ni or Co) composites", Materials Letters 59 (2005) 2647-2649.

[15] M. Shafiei, A.T. Alpas, "Effect of sliding speed on friction and wear behaviour of nanocrystalline nickel tested in an argon atmosphere", Wear **265** (2008) 429–438.

[16] R. Karslioglu, H. Akbulut, "Comparison microstructure and sliding wear properties of nickel–cobalt/CNT composite coatings by DC, PC and PRC current electro deposition", Applied Surface Science 353 (2015) 615–627.

[17] H. Algu, M. Tokur, S. Ozcan, M. Uysal, T. Cetinkaya, H. Akbulut, A. Alp, "The effect of graphene content and sliding speed on the wear mechanism of nickel-graphene nanocomposites", Applied Surface Science **359** 340–348 (2015).

[18] C. Dellacorte & J. A. Laskowski (1997), "Tribological Evaluation of PS300: A New Chrome Oxide-Based Solid Lubricant Coating Sliding Against Al2O3 from 25° to 650°C", Tribology Transactions, 40:1, 163-167, DOI: 10.1080/10402009708983642.

[19] C. DellaCorte and B.J. Edmonds, "NASA PS400: A New High Temperature Solid Lubricant Coating for High Temperature Wear Applications", NASA/TM—2009-215678.

[20] J. Zhen, S. Zhu, J. Cheng, Z. Qiao, W. Liu, J. Yang, "Effects of sliding speed and testing temperature on the tribological behavior of a nickel- alloy based solid-lubricating composite", Wear **368-369** (2016) 45–52.

**CHAPTER V**

[1] J. Nelson (2017), "Synthesis and Characterization of MAX Ceramics (MAXCERs)" (Masters Thesis), ProQuest Dissertations and Theses, Publication Number: AAT 10616046; ISBN: 9780355432688.

[2] M.W. Barsoum and T. El-Raghy, "Synthesis and Characterization of a Remarkable Ceramic: $Ti_3SiC_2$", Journal of the American Ceramic Society, 79, 1953-1956 (1996).

[3] S. Gupta and M.W. Barsoum, "On the tribology of the MAX phases and their composites during dry sliding: A review", Wear, 271, 1878-1894 (2011).

[4] S. Gupta, D. Filimonov, V. Zaitsev, T. Palanisamy, and M.W. Barsoum, "Ambient and 550 °C tribological behavior of select MAX phases against Ni-based superalloys", Wear, (2007).

[5] S. Gupta, D. Filimonov, T. Palanisamy, and M.W. Barsoum, "Tribological behavior of select MAX phases against $Al_2O_3$ at elevated temperatures", Wear, 265, 560-565 (2008).